Available online at www.sciencedirect.com
ScienceDirect
Lithos 90 (2006) 249–270
LITHOS
www.elsevier.com/locate/lithos

Geochemistry and petrology of Tertiary volcanic rocks and related ultramafic xenoliths from the central and eastern Oman Mountains

Sobhi Nasir *, Abdulrazak Al-Sayigh, Abdulrahman Alharthy, Ali Al-Lazki

Department of Earth Science, Sultan Qaboos University, PO Box 36, 123 Al-Khod, Sultanate of Oman

Received 18 June 2005; accepted 10 March 2006
Available online 18 May 2006

Abstract

The Tertiary volcanic rocks of the central and the eastern parts of the Oman Mountains consist mainly of basanites with abundant upper mantle ultramafic xenoliths. The lavas are alkaline (42–43 wt.% SiO_2; 3.5–5.5 wt.% Na_2O+K_2O). They include primitive (11–14 wt.% MgO) features with strong OIB-like geochemical signatures. Trace element and Sr–Nd isotope data for the basanites suggest mixing of melts derived from variable degrees of melting of both garnet- and spinel lherzolite-facies mantle source. The associated xenolith suite consists mainly of spinel and Cr-bearing diopside wehrlite, lherzolite and dunite with predominantly granuloblastic textures. No significant difference in chemistry was found between the basanites and xenoliths from the central and eastern Oman Mountains, which indicate a similar mantle source. Calculated oxygen fugacity indicates equilibration of the xenoliths at −0.43 to −2.2 log units above the fayalite–magnetite–quartz (FMQ) buffer. Mantle xenolith equilibration temperatures range from 910–1045+50 °C at weakly constrained pressures between 13 and 21 kbar. Xenolith data and geophysical studies indicate that the Moho is located at a depth of ~40 km. A geotherm substantially hotter (90 mW m^{-2}) than the crust–mantle boundary (45 mW m^{-2}) is indicated and probably relates to tectonothermal events associated with the local and regional Tertiary magmatism. The petrogenesis of the Omani Tertiary basanites is explained by partial melting of an asthenospheric mantle protolith during an extension phase predating opening of the Gulf of Aden and plume-related alkaline volcanic rocks.
Published by Elsevier B.V.

Keywords: Basanite; Oman Mountains; Ultramafic xenoliths; Geochemistry; Extension; Mantle plume; Lithosphere; P-T conditions

1. Introduction

Mafic and ultramafic xenoliths from basaltic rocks yield information on the nature of the lithosphere and the generation of basaltic magma from the mantle (e.g., Griffin and O'Reilly, 1987; Rudnick, 1992; Kempton et al., 1997; Vannucci et al., 1998; Eggins et al., 1998; Griffin et al., 1999; Neumann et al., 2002; Ionov et al., 2005; Gautheron et al., 2005). The xenoliths can offer direct evidence of the composition of the lower crust and upper mantle used for modelling. The Tertiary volcanic province of the Arabian plate has provided a major impetus for plume models to explain the formation of continental flood basalt (Stein and Hoffman, 1992; Stein and Goldstein, 1996; Laws and Wislon, 1997; Stein et al., 1997). The relative importance of plume mantle versus lithospheric mantle in the extension related to alkaline magmatism has been the key issue in recent investigations of intraplate volcanism (Simonetti et al., 1998; Trumbull et al., 2003; Karamalkar et al., 2005).

* Corresponding author.
E-mail addresses: sobhi@squ.edu.om (S. Nasir), alsayigh@squ.edu.om (A. Al-Sayigh), abuali@squ.edu.om (A. Alharthy), lazki@squ.edu.om (A. Al-Lazki).

0024-4937/$ - see front matter. Published by Elsevier B.V.
doi:10.1016/j.lithos.2006.03.002

Ultramafic xenolith bearing Tertiary basanites are found near Muscat, central part of the Oman Mountains (Al-Harthy et al., 1991; Gnos and Peters, 2003). Several workers mentioned also the occurrence of small Tertiary basanite intrusions near the Ashkharah area within the Batain Nappes of southeastern Oman (Fig. 1) (e.g., Shackleton et al., 1990; Béchennec et al., 1992; Peters et al., 2001; Worthing and Wilde, 2002; Gnos and Peters, 2003). The Tertiary basanites of Oman contain commonly mantle xenoliths. Worthing and Wilde (2002) related the Tertiary basanite intrusions in the southeastern parts of Oman to the Tertiary tectonism and major

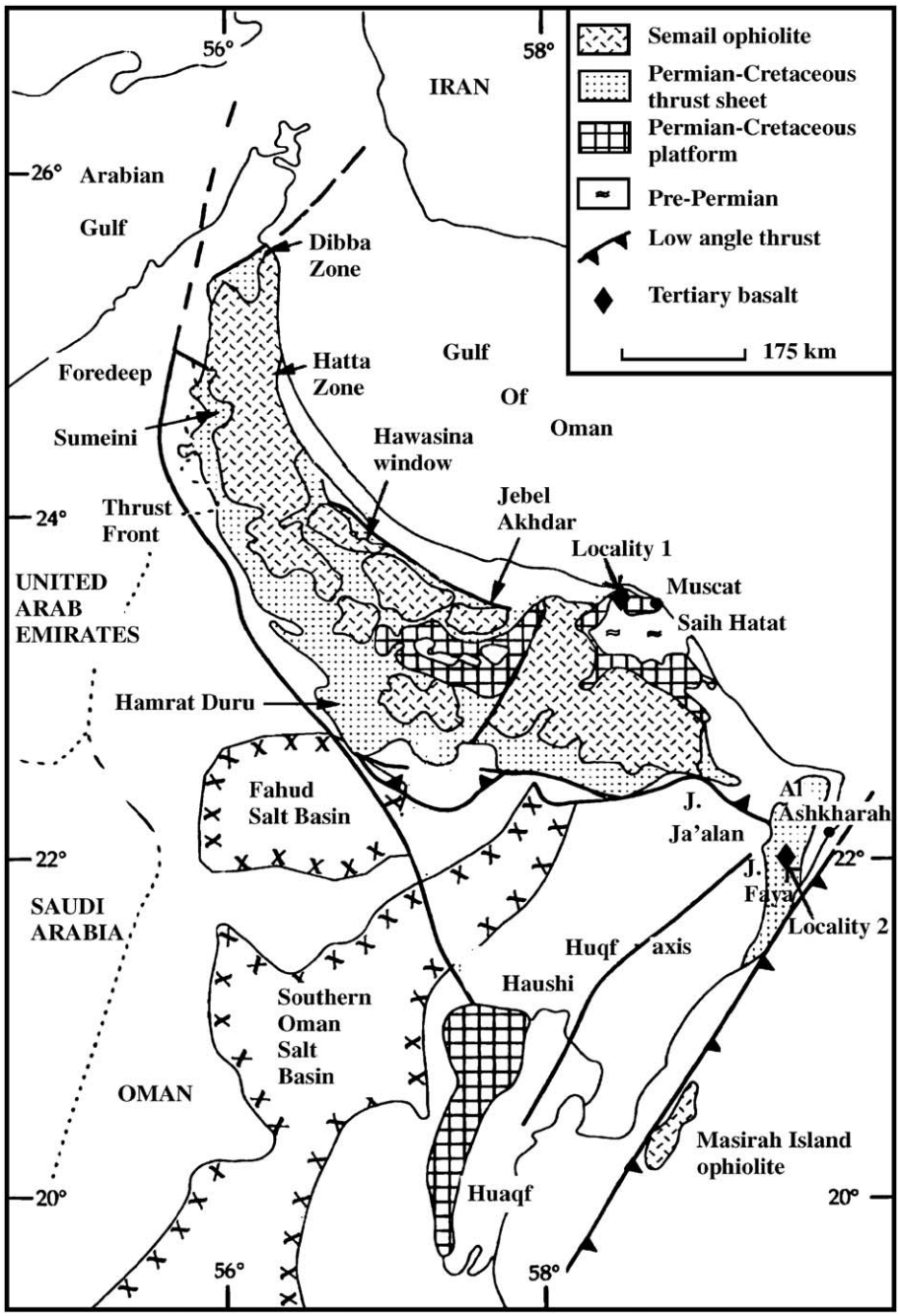

Fig. 1. Structural sketch map of the Oman Mountains showing the main tectonic units and location of the study area (after Robertson and Searle, 1990).

uplift of the Oman Mountain range. However, Carbon (1996) indicates absence of regional tectonic extension in the Eocene for Oman. According to Filbrandt et al. (1990) the main Jebel Ja'alan (eastern Oman) uplift seems end-Maastrichtian/Paleocene in age but not Eocene.

Little has been published on the basanites and xenoliths from Oman. In comparison, lithospheric compositions beneath the northern and western parts of the Arabian plate are known in detail (e.g., McGuire, 1988a,b; Nasir, 1992, 1994, 1995, 1996; Nasir and Al-Fuqha, 1988; Nasir and Mahmood, 1991; Nasir and Safarjalani, 2002; Nasir et al., 1992, 1993; Al-Mishwat and Nasir, 2003). In addition to published data on the basanites of southeastern part of Oman (Peters et al., 2001; Worthing and Wilde, 2002; Gnos and Peters, 2003) the present data on Tertiary basanites and associated ultramafic xenoliths from the central and southeastern parts of Oman provide new insight into the petrology and geochemistry of the lithosphere underneath Oman.

2. Geological setting

The tectonically emplaced Semail ophiolite and associated Hawasina sediments are unconformably overlain by a Maastrichtian and lower Tertiary shelf sequence. This cover sequence has been deformed in mid to late Tertiary events associated with the major uplift of the Oman mountain range (Hanna, 1990; Nolan et al., 1990; Mann et al., 1990; Carbon, 1996). Tertiary volcanic rocks are confined to the extreme eastern corner of Oman around the Jebel Ja'alan basement block. In general Tertiary magmatic activity was closely related to major fracture zones (Nolan et al., 1990; Gnos and Peters, 2003). Small basanitic intrusions were emplaced along N–S and E–W lineaments within the Batain Nappes, which form the northerly extension of the Eastern Ophiolite Complex (Masirah Ophiolite) (Shackleton et al., 1990; Immenhauser et al., 1998; Worthing and Wilde, 2002; Gnos and Peters, 2003). The N–S and E–W lineaments parallel the major tectonic structure in the region. Both lineaments are probably reactivated older fault systems (Peters et al., 2001). Mantle xenoliths on which this study is based are hosted in Tertiary basanite dykes exposed near Muscat, central part of the Oman Mountains (Al-Harthy et al., 1991) and in several intrusive plugs near Jebel Faya, Al Ashkharah area, eastern Oman (locality 1 and 2 respectively, Fig. 1). The basanites contain abundant fine to medium-grained ultramafic xenoliths (0.5–2 cm in diameter). The basanitic rocks near Muscat are found as small cluster of dykes 20–50 m in diameter, cutting the lower part of the Paleocene sequence (Jafnayn Formation) as well as the Maastrichtian Al-Khod conglomerate Formation (Al-Harthy et al., 1991). The age of the youngest country rock hosting these basanite dykes is Paleocene and this provides a minimum age for the basanites in Muscat area. The basanites occur on the eastern limb of a synform where the contact of the Jafnayn Formation and the Al-Khod Formation is a N–S normal fault.

Renewed extension of the central and eastern Oman Mountains in Late Paleocene resulted in formation of the NNW–SSE trending Abat trough, which is bounded to the south by the north Ja'alan fault and to the east by the Qahalt fault (Wyns et al., 1992). Most of the basanitic intrusions in the eastern Oman Mountains define an E–W or a N–S trending lineament that is sub parallel to the Qahalt fault (Fig. 1). Whole rock Ar/Ar age determinations on these basanites range from 36 to 44 Ma (Ries et al., 1985; Worthing and Wilde, 2002). These ages are older than those of Tertiary basalts of Saudi Arabia, Yemen and Jordan, which are related to the opening of the Red Sea and the Gulf of Aden (Camp and Roobol, 1989; Camp et al., 1991, 1992; Nasir, 1994; Baker et al., 1997).

3. Analytical methods

Mineral analyses were carried out at Universität Stuttgart using the wavelength-dispersive system of a CAMECA SX100 electron microprobe. Operating conditions were: 15 kV accelerating voltage, 10 to 15 nA beam current and an integration time of 20 s on peak and on background. The raw data were corrected using the PAP procedure. Three to eight spots were analyzed on each grain. Major elements (Si, Ti, Al, Fe, Mn, Mg, Ca, Na, K, and P) were analyzed by standard X-ray fluorescence techniques (Philips PW 2400 XRF), except for Na, which was determined by AAS. Trace and REE elements were analyzed by inductively coupled plasma-mass spectrometry (Agilent 7500 ICPMS) using the preparation techniques of Jenner et al. (1990). About 200 mg of powdered sample was weighed in screw-top Teflon autoclaves. The samples were dissolved in a $HF–HNO_3$ mixture, evaporated to dryness on a hot plate. The cycle of acid addition and drying was repeated 3 or 4 times. To insure complete dissolution, $HCLO_4$ was added during the evaporation stage. Millipore-filtered distilled water was then added. The solution was spiked with 100 ppm Ag and Ta. Three aliquots of the spiked solution were analyzed on the ICP-MS. Multi-element standards and USGS standards were used to calibrate the ICP-MS. The precision is estimated to be 4–6% of the reported results.

Table 1
Modal mineralogy of peridotite mantle xenolithsin Tertiary basanites from Oman

Sample	Lithology	Ol	Cpx	Opx	Sp
Central Oman (Muscat, locality 1)					
Md-1	Sp-dunite	91	6	2	1
Md-2		92	5	2	1
Ml-1	Sp-lherzolite	79	14	6	1
Ml-2		76	15	8	1
Mw-3	Sp-wehrlite	78	18	3	1
Eastern Oman (Al Ashkharah, locality 2)					
Ad-1	Sp-dunite	91	7	1	1
Ad-2		91	5	3	1
Aw-1	Sp-wehrlite	84	14	1	1
Aw-2		82	14	3	1
Aw-3		85	13	1	1

Ol: olivine, Cpx: clinopyroxene, Opx: orthopyroxene, Sp: spinel.

The basanite samples from Muscat area were analyzed for Sr–Nd isotopes in the Analytical Geochemistry Laboratories of the British Geological Survey. Samples for Sm–Nd analysis were spiked with ^{150}Nd and ^{147}Sm isotopically enriched tracers and decomposed using HF in sealed teflon bombs at 120 °C. Following treatment with HNO_3 and conversion to the chloride form with 6 M HCl, Sr and the REE were separated by standard ion exchange procedures using Biorad AG50W-X8 ion exchange resin. Sm and Nd were separated from the REE fraction by reverse phase ion chromatography on a column filled with Biobeads coated with di-2-ethylhexyl orthophosphoric acid (HDEHP). The procedural blank for Nd was 500 pg. Isotope ratio measurements were made on a Finnegan-MAT 262 mass spectrometer at the NERC Isotope Geosciences Laboratory. Errors are quoted throughout as two standard deviations from the measured or calculated values. Analytical uncertainties are estimated to be ±0.01% for $^{143}Nd/^{144}Nd$ and $^{87}Sr/^{86}Sr$ ratios. Measured $^{143}Nd/^{144}Nd$ were corrected for mass fractionation relative to $^{146}Nd/^{144}Nd=0.7219$, and $^{87}Sr/^{86}Sr$ ratios relative to $^{86}Sr/^{88}Sr=0.1194$. Replicate analyses ($n=29$) of a Johnson and Matthey Nd standard made during the period of analysis yielded a mean $^{143}Nd/^{144}Nd$ of 0.511188+0.000024. This is equivalent to a value of 0.511923 for the La Jolla international Nd isotope standard. The average $^{87}Sr/^{86}Sr$ determined for the NBS 987 strontium isotope standard was 0.710250+0.000028 ($n=24$).

4. Petrography

4.1. Basanite

The basanitic rocks are dark colored, compact and occasionally contain vesicles. They are fine-grained and micoporphyritic, containing 20% to 30% sub to euhedral olivine and clinopyroxene phenocrysts with

Table 2
Representative microprobe analysis of olivine

Area	Muscat							Al Ashkharah				
Rock	Dunite		Lherzolite		Wehrlite	Basanite		Dunite		Wehrlite		
						Core	Rim					
Sample	Md-1	Md-2	Ml-1	Ml-2	Mw-3	Mb-1		Ad-1	Ad-2	Aw-1	Aw-2	Aw-3
SiO_2	40.92	40.98	40.8	40.75	40.95	39.98	39.64	40.92	41.03	41.4	40.95	41.20
Cr_2O_3	0.03	0.02	0.03	0.02	0.02	0.00	0.00	0.01	0.01	0.02	0.01	0.01
FeO	9.11	8.91	9.30	9.15	9.20	13.14	13.46	9.43	9.38	9.85	9.55	9.45
NiO	0.42	0.41	0.40	0.42	0.40	0.00	0.00	0.39	0.41	0.42	0.41	0.39
MnO	0.06	0.08	0.10	0.13	0.10	0.20	0.20	0.32	0.20	0.13	0.22	0.18
MgO	49.22	49.65	49.15	49.32	49.25	46.34	45.88	49.31	49.45	48.95	49.12	49.25
CaO	0.04	0.05	0.05	0.04	0.04	0.20	0.30	0.04	0.05	0.05	0.04	0.04
Total	99.8	100.1	99.83	99.83	99.96	99.86	99.48	100.2	100.43	100.55	100.18	100.44
Mg#	0.90	0.90	0.90	0.90	0.90	0.86	0.85	0.90	0.90	0.89	0.90	0.90
Cations on the basis of 4 oxygen and 3 cations pfu												
Si	1.001	0.999	0.999	0.998	1.001	0.997	0.995	0.999	0.999	1.002	1.000	1.003
Cr	0.001	0.000	0.001	0.000	0.000	0.000	0.000	0.000	0.000	0.000	0.000	0.000
Fe^{2+}	0.186	0.182	0.190	0.187	0.188	0.274	0.282	0.193	0.191	0.201	0.195	0.192
Ni	0.013	0.013	0.012	0.013	0.012	0.000	0.000	0.012	0.013	0.013	0.013	0.012
Mn	0.001	0.002	0.002	0.003	0.002	0.004	0.004	0.002	0.002	0.002	0.002	0.002
Mg	1.796	1.803	1.794	1.798	1.795	1.794	1.723	1.716	1.795	1.778	1.789	1.787
Ca	0.001	0.001	0.001	0.001	0.001	0.005	0.008	0.001	0.001	0.001	0.001	0.001
Total	3.000	3.000	3.000	3.000	3.000	3.003	3.005	3.000	3.000	3.000	3.000	3.000

oscillatory zoning patterns. Groundmass textures are microcrystalline and vary between vitrophyric, intersertal and intergranular with subhedral olivine, lath-like pinkish clinopyroxene, plagioclase, nepheline, sanidine and Ti-magnetite as the dominant phases. Detailed descriptions are given by Al-Harthy et al. (1991), Worthing and Wilde (2002) and Gnos and Peters (2003).

4.2. Xenoliths

Mantle xenoliths are green in color, rounded or elongated and 0.5 to 2 cm in diameter. The xenoliths sampled from the Muscat area are spinel wehrlite, spinel lherzolite and spinel dunite, whereas those from Al Ashkharah area are spinel wehrlite and spinel dunite. The modal proportions of the mineral phases as determined from bulk composition are given in Table 1. The xenoliths are dominated by 0.2 to 0.5 mm-sized olivine and clinopyroxene. Small sized xenoliths (<1 cm in diameter) show granuloblastic texture and display weak foliation. Larger xenoliths may show clear foliation. Olivine neoblasts (<0.5 mm in diameter) in the dunite xenoliths have straight planar to gently curved boundaries, forming commonly 120° triple junctions. Some grains display dislocation walls and undulose extinction. In wehrlite and in lherzolite olivine mainly forms deformed <0.5 mm grains, but also forms inclusion in clinopyroxene. Clinopyroxene is commonly poikilitic, it forms anhedral grains (0.3 mm in diameter in dunite and ~0.5 mm in lherzolite and wehrlite) enclosing round grains of olivine and orthopyroxene and irregular to vermicular brown spinel. Orthopyroxene and brown spinel are minor (<5 vol.%). Spinel is mostly interstitial and typically brown holly leaf-shaped. Orthopyroxene forms small interstitial grains in neoblast areas, and

Table 3
Representative microprobe analysis of clinopyroxene

Area	Muscat							Al Ashkharah				
Rock	Dunite		Lherzolite		Wehrlite	Basanite		Dunite		Wehrlite		
						Core	Rim					
Sample	Md-1	Md-2	Ml-1	Ml-2	Mw-3	Mb-1		Ad-1	Ad-2	Aw-1	Aw-2	Aw-3
SiO_2	53.1	52.8	52.8	52.85	52.71	49.62	49.78	52.95	53.08	53.21	53.1	52.98
TiO_2	0.14	0.12	0.11	0.11	0.07	1.30	1.14	0.15	0.08	0.13	0.11	0.12
Al_2O_3	4.18	4.52	4.06	4.22	4.54	7.10	8.46	4.32	4.14	4.25	4.25	4.42
Cr_2O_3	0.36	0.42	0.33	0.38	0.34	0.07	0.04	0.21	0.33	0.25	0.36	0.30
Fe_2O_3	0.74	0.51	0.95	0.51	0.55	2.89	1.74	0.92	0.30	0.39	0.50	0.33
FeO	1.71	2.14	2.07	2.19	2.51	2.22	3.37	2.07	2.48	2.53	2.50	2.80
NiO	–	0.01	–	0.02	–	–	–	0.01	0.01	0.01	0.01	0.01
MnO	0.05	0.10	0.15	0.10	0.08	0.13	0.06	0.10	0.08	0.10	0.1	0.12
MgO	16.48	16.62	17.21	16.24	17.14	15.20	14.65	16.39	16.25	16.15	16.31	16.05
CaO	21.66	21.41	21.24	22.05	21.11	21.29	22.13	21.35	21.81	21.45	21.34	21.55
Na_2O	1.02	0.85	0.67	0.81	0.63	0.82	1.11	1.01	0.85	1.04	0.98	0.92
Total	99.44	99.50	99.59	99.48	99.68	100.64	100.75	99.48	99.41	99.51	99.56	99.60
Mg#	0.92	0.91	0.91	0.91	0.91	0.83	0.80	0.90	0.90	0.90	0.90	0.90
Cations on the basis of 6 oxygen and 4 cations pfu												
Si	1.927	1.917	1.917	1.923	1.911	1.801	1.800	1.924	1.926	1.933	1.929	1.926
Al	0.179	0.193	0.174	0.181	0.194	0.304	0.295	0.185	0.190	0.182	0.182	0.189
Ti	0.004	0.003	0.003	0.003	0.002	0.035	0.031	0.004	0.002	0.004	0.003	0.003
Cr	0.010	0.012	0.009	0.011	0.010	0.002	0.001	0.006	0.005	0.007	0.010	0.009
Fe^{3+}	0.020	0.014	0.026	0.014	0.015	0.079	0.054	0.025	0.005	0.011	0.014	0.009
Fe^{2+}	0.052	0.065	0.063	0.067	0.076	0.067	0.107	0.063	0.078	0.077	0.076	0.085
Ni	0.000	0.000	0.000	0.001	0.000	0.000	0.000	0.000	0.000	0.000	0.000	0.000
Mn	0.002	0.003	0.005	0.003	0.002	0.004	0.002	0.003	0.002	0.003	0.003	0.004
Mg	0.892	0.900	0.931	0.881	0.926	0.822	0.793	0.888	0.879	0.875	0.883	0.870
Ca	0.842	0.833	0.826	0.860	0.820	0.828	0.779	0.831	0.848	0.835	0.831	0.839
Na	0.072	0.060	0.046	0.056	0.044	0.058	0.078	0.071	0.060	0.072	0.068	0.064
Total	4.000	4.000	4.000	4.000	4.000	4.000	4.000	4.000	4.000	4.000	4.000	4.000
Wo	46.60	46.00	44.60	47.10	44.60	45.90	46.80	46.40	45.90	46.40	46.00	45.00
En	49.30	49.60	50.30	48.30	50.30	49.10	48.50	48.60	48.90	48.20	45.70	45.80
Fs	4.10	4.40	5.10	4.60	5.10	5.00	4.70	5.00	5.20	5.40	8.30	9.10

blebs inside clinopyroxenes. Hydrous minerals, such as amphibole and phlogopite, are absent.

5. Mineral chemistry

The mineral chemistry of the xenoliths from both localities is indistinguishable. Olivine falls within the range $Fo_{89–90}$ and NiO contents ranges between 0.39–0.42 (Table 2), typical for the type I xenoliths in the world (Frey and Prinz, 1978). Magmatic olivine phenocrysts in the associated basanite have Mg-rich cores ($Fo_{80–82}$) and Fe-rich rims ($Fo_{76–78}$).

The clinopyroxene in the xenoliths also has a limited composition ($Wo_{44.6–50.3}En_{48.2–50.3}Fs_{4.1–5.4}$) in all xenoliths (Table 3). Clinopyroxene in host basanites is richer in TiO_2, FeO, Al_2O_3 and tends toward lower MgO, Cr_2O_3 and Na_2O contents than clinopyroxene in the xenoliths. The host basanite clinopyroxene has a composition of $Wo_{6.0}En_{45.7}Fs_{8.3}$. Compositional zoning with increasing Fe and Al, and decreasing Mg, Cr and Ca, from core to rim is common in clinopyroxene of the host basanite but is uncommon in those of xenoliths.

Orthopyroxene shows also a restricted range in composition varying from $En_{90}Fs_{10}$ to $En_{93}Fs_7$ in all xenolith's types (Table 4). The spinel has characteristically moderate to high Cr_2O_3 contents (16.0–21.0 wt. %) and low Al_2O_3 (46.5–50.2 wt.%) and falls within the range of chrom-spinel (Table 5). Groundmass plagioclase in basanite has composition ranging from andesine to labradorite ($An_{42–60}$, Table 6). Sanidine shows a compositional range of $Ab_{39–48}An_{4–5}Or_{48–56}$ and nepheline has a composition of $Ne_{82}Ks_{18}$ (Table 6).

6. Geochemistry

6.1. Basanite

The major and trace element concentrations of the investigated basanites from Muscat area are given in

Table 4
Representative microprobe analysis of orthopyroxene

Area	Muscat					Al Ashkharah				
Rock	Dunite		Lherzolite		Wehrlite	Dunite		Wehrlite		
Sample	Md-1	Md-2	Ml-1	Ml-2	Mw-3	Ad-1	Ad-2	Aw-1	Aw-2	Aw-3
SiO_2	55.60	55.63	55.22	55.32	55.25	55.52	55.40	55.50	55.2	55.6
TiO_2	0.04	0.06	0.05	0.03	0.05	0.02	0.04	0.07	0.05	0.04
Al_2O_3	4.31	3.90	4.15	4.34	4.48	4.40	4.18	3.89	4.03	3.79
Cr_2O_3	0.05	0.05	0.10	0.10	0.10	0.15	0.12	0.50	0.10	0.08
Fe_2O_3	0.44	0.53	0.52	0.45	0.38	0.41	0.23	0.21	0.78	0.26
FeO	5.51	5.37	6.08	5.74	5.51	5.98	5.74	6.25	5.49	5.99
NiO	–	0.01	–	0.01	0.01	0.0	0.05	0.0	0.01	0.01
MnO	0.08	0.08	0.11	0.15	0.10	0.15	0.21	0.13	0.10	0.08
MgO	33.30	33.58	32.88	32.97	33.25	32.9	32.95	32.87	33.05	33.18
CaO	0.82	0.78	0.69	0.76	0.76	0.73	0.78	0.73	0.68	0.71
Na_2O	0.10	0.05	0.09	0.1	0.05	0.15	0.10	0.10	0.13	0.08
Total	100.25	100.04	99.89	99.97	99.94	100.41	99.8	100.25	99.62	99.82
Mg#	0.91	0.91	0.90	0.90	0.91	0.90	0.90	0.91	0.90	0.90
Cations on the basis of 6 oxygen and 4 cations pfu										
Si	1.909	1.914	1.909	1.908	1.903	1.908	1.913	1.914	1.910	1.920
Al	0.174	0.158	0.001	0.176	0.182	0.178	0.170	0.158	0.164	0.154
Ti	0.001	0.002	0.169	0.001	0.001	0.001	0.001	0.002	0.001	0.001
Cr	0.001	0.001	0.003	0.003	0.003	0.004	0.003	0.014	0.003	0.002
Fe^{3+}	0.011	0.014	0.013	0.012	0.010	0.011	0.006	0.006	0.020	0.007
Fe^{2+}	0.158	0.155	0.175	0.166	0.159	0.172	0.166	0.180	0.159	0.173
Ni	0.000	0.000	0.000	0.000	0.000	0.000	0.002	0.000	0.000	0.000
Mn	0.002	0.002	0.003	0.004	0.003	0.004	0.006	0.004	0.003	0.002
Mg	1.705	1.722	1.695	1.695	1.708	1.685	1.696	1.689	1.705	1.708
Ca	0.030	0.029	0.026	0.028	0.028	0.027	0.029	0.027	0.025	0.026
Na	0.006	0.002	0.006	0.006	0.002	0.010	0.006	0.006	0.008	0.004
Total	4.000	4.000	4.000	4.000	4.000	4.000	4.000	4.000	4.000	4.000
En	0.92	0.93	0.90	0.91	0.91	0.91	0.91	0.90	0.91	0.91
Fs	0.08	0.07	0.10	0.09	0.09	0.09	0.09	0.10	0.09	0.09

Table 5
Representative microprobe analysis of spinel

Area	Muscat					Al Ashkharah				
Rock	Dunite		Lherzolite		Wehrlite	Dunite		Wehrlite		
Sample	Md-1	Md-2	Ml-1	Ml-2	Mw-3	Ad-1	Ad-2	Aw-1	Aw-2	Aw-3
SiO_2	0.05	0.10	0.04	0.06	0.05	0.03	0.08	0.02	0.03	0.02
TiO_2	0.04	0.09	0.13	0.03	0.01	0.06	0.11	0.20	0.02	0.03
Al_2O_3	49.04	50.06	48.73	47.20	48.12	49.5	50.18	48.8	47.82	46.55
Cr_2O_3	17.38	16.03	18.05	20.05	18.31	18.86	17.13	19.55	20.21	21.05
Fe_2O_3	3.95	4.65	3.34	3.53	4.72	2.33	2.81	2.41	2.77	3.63
FeO	9.59	7.93	9.90	9.05	7.80	8.16	9.20	8.23	9.13	8.42
NiO	0.14	0.21	0.23	0.20	0.18	0.10	0.18	0.20	0.15	0.13
MnO	0.32	0.24	0.23	0.15	0.30	0.32	0.20	0.13	0.22	0.18
MgO	19.42	20.68	19.2	19.65	20.45	20.41	19.88	20.45	19.65	20.02
Total	99.93	99.99	99.84	99.92	99.94	99.77	99.77	99.99	99.99	100.05
Mg#	0.72	0.76	0.72	0.74	0.76	0.77	0.74	0.77	0.74	0.75
Cr#	0.19	0.18	0.20	0.22	0.20	0.20	0.19	0.21	0.22	0.23
Cations on the basis of 4 oxygen and 3 cations pfu										
Si	0.001	0.003	0.001	0.002	0.001	0.001	0.002	0.001	0.001	0.001
Ti	0.001	0.002	0.003	0.001	0.000	0.001	0.002	0.004	0.004	0.001
Al	1.548	1.513	1.542	1.497	1.515	1.553	1.574	1.531	1.513	1.475
Cr	0.368	0.336	0.383	0.427	0.387	0.397	0.361	0.411	0.429	0.448
Fe^{3+}	0.080	0.093	0.067	0.072	0.095	0.047	0.056	0.048	0.056	0.074
Fe^{2+}	0.215	0.176	0.222	0.204	0.174	0.182	0.205	0.183	0.205	0.190
Ni	0.005	0.007	0.008	0.007	0.006	0.003	0.006	0.007	0.005	0.004
Mn	0.007	0.005	0.005	0.003	0.007	0.007	0.005	0.003	0.005	0.004
Mg	0.775	0.816	0.768	0.788	0.814	0.810	0.789	0.812	0.786	0.803
Total	3.000	3.000	3.000	3.000	3.000	3.000	3.000	3.000	3.000	3.000

Table 7. The lavas are alkaline series of volcanics (most have 8–13 normative nepheline; 42–43 wt.% SiO_2; 3.5–5.5 Na_2O+K_2O), with almost all samples plotting in the basanite fields on a total alkali–silica classification diagram (Fig. 2) and SiO_2 versus Zr/TiO_2 diagram (Fig. 3). However, they are less alkaline than other equivalent Neogene lavas from the Al Ashkharah area (locality 2). The lavas have relatively high Mg#s (0.70–0.72) and Cr (380–440 ppm) and Ni (320–410 ppm) (Table 1) that support the idea that these lavas have suffered only moderate amounts of crystal fractionation from primitive, mantle-derived basanites.

Primitive mantle-normalized trace element patterns are shown in Fig. 4. There is virtually no difference between the trace element patterns of samples from the Muscat area and those of the Al Ashkharah area. The patterns generally dip with increasing element incompatibility. These patterns are similar to that of the average oceanic island basalt (Sun and McDonough, 1989).

Fig. 5 summarizes the trace element contents of the Omani basanites in a multi-element diagram normalized to an average composition of ocean island basalts (Sun and McDonough, 1989). This underlines the similarity between the Omani basanitic rocks and the OIB suite. Omani basanites have higher Ba, Th and Sr and slightly lower Zr, Y and Ti than OIB. The negative troughs of K and Rb may be related to retention of phlogopite and/or amphibole in the source during melting (e.g., Wilson and Downes, 1991), or due to liquid immiscibility (e.g., Gnos and Peters, 2003). In the Y versus Zr plot (Fig. 6) most basanite samples have $Zr/Y=8.7–10$ and plot on the ocean island basalt (OIB) line.

The chondrite-normalized REE patterns of basanites from Oman are shown in Fig. 7. They have smooth slopes with LREE enrichment (150–200 times chondrite) and do not show significant positive Eu and Ce anomalies. This suggests either sufficiently high oxygen fugacities so that Eu is trivalent and hence not entering the plagioclase structure, or negligible fractionation of plagioclase, which is in keeping with the lack of plagioclase in the phenocryst assemblage. All of the samples, regardless of location, show similar chondrite-normalized REE patterns. Heavy REE abundances are ca 6 times chondrite suggesting that partial melting may have occurred at relatively deep depths.

The Tertiary basanites of central Oman show a restricted range in Sr and Nd isotopic composition ($^{87}Sr/$

Table 6
Representative microprobe analysis of feldspar in basanite

Area	Muscat								
Sample	Mb-1	Mb-2	Mb-3	Mb-4	Mb-5	Mb-6	Mb-3	Mb-5	Mb-3
Mineral	plg	plg	plg	plg	plg	plg	sdn	sdn	ne
SiO_2	53.47	54.18	52.85	56.95	54.28	531.5	64.96	64.38	41.85
TiO_2	0.10	0.05	0.02	0.12	0.08	0.14	0.06	0.05	0.02
Al_2O_3	29.46	28.94	29.76	26.85	29.15	29.55	19.71	19.97	35.58
Fe_2O_3	0.33	0.40	0.25	0.35	0.32	0.28	0.40	0.36	0.04
CaO	12.05	11.33	12.35	8.68	11.11	11.88	0.65	0.99	2.14
Na_2O	4.51	4.75	4.38	6.31	4.92	4.41	5.43	4.39	15.83
K_2O	0.42	0.55	0.33	0.54	0.43	0.51	8.38	9.67	5.24
Total	100.34	100.2	99.94	99.80	100.29	99.92	99.39	99.73	100.71
Cations on the basis of 8 oxygen							*4 oxygen*		
Si	2.415	2.447	2.398	2.564	2.446	2.410	2.941	2.925	0.998
Ti	0.003	0.002	0.001	0.004	0.003	0.005	0.002	0.002	0.001
Al	1.568	1.540	1.591	1.425	1.548	1.579	1.052	1.071	1.000
Fe^{3+}	0.011	0.013	0.009	0.012	0.011	0.010	0.014	0.012	0.001
Ca	0.583	0.548	0.600	0.419	0.536	0.577	0.036	0.048	0.055
Na	0.395	0.416	0.385	0.551	0.430	0.388	0.477	0.387	0.732
K	0.024	0.032	0.019	0.031	0.025	0.030	0.484	0.561	0.159
Total	5.001	4.998	5.003	5.005	4.999	5.000	5.005	5.006	2.946
Ab	0.58	0.55	0.60	0.42	0.54	0.58	0.48	0.39	
An	0.40	0.42	0.38	0.55	0.43	0.39	0.04	0.05	
Or	0.02	0.03	0.02	0.03	0.03	0.03	0.48	0.56	
Ne									0.82
Ks									0.18

plg; plagioclase, sdn; sanidine, ne; nepheline.

$^{86}Sr = 0.704003–0.704177$, $^{143}Nd/^{144}Nd = 0.512719–0.512783$; Table 7). Worthing and Wilde analyzed the Tertiary basanites of southeast Oman and obtained $^{87}Sr/^{86}Sr = 0.70336–0.70426$; $^{143}Nd/^{144}Nd = 0.512821–0.512914$. Sr–Nd isotopic data for Cenozoic intraplate volcanic rocks from the Arabian plate (Altherr et al., 1990; Henjes-Kunst et al., 1990; Schilling et al., 1992; Baker et al., 1997; Volker et al., 1997; Hopp et al., 2004) are included in the comparison with the Omani Cenozoic basanites in Fig. 8.

6.2. Xenolith

Chemical compositions of the xenoliths are listed in Table 8. For comparison, the composition of the primitive upper mantle (PUM) as estimated by Jagoutz et al. (1979) is added. The dunite, lherzolite and wehrlite xenoliths are highly refractory with respect to TiO_2 and Al_2O_3 (dunite: 0.02–0.07 wt.% TiO_2, 0.55–0.72 wt.% Al_2O_3; lherzolite and wehrlite: 0.14–0.19 wt.% TiO_2, 0.63–1.03 wt.% Al_2O_3). The dunite, lherzolite and wehrlite have mg-numbers of 0.89–0.90 and show a wide range in CaO concentrations (1.06–1.6 in dunite and 2.70–3.87 wt.% in lherzolite and wehrlite). Silica is moderately depleted (41–43 wt.%) and MgO is slightly enriched (up to 47 wt.%) as compared to PUM (38.3 wt.%).

Primitive mantle-normalized trace element patterns (Fig. 9) resemble those of lherzolite xenoliths from Group I xenoliths of the Arabian plate (McGuire, 1988a, b; Nasir and Al-Fuqha, 1988; Nasir, 1992) and peridotite worldwide (e.g., McDonough and Frey, 1989).

Chondrite normalized patterns are shown in Fig. 10. The dunite xenoliths are characterized by low, almost chondritic HREE and MREE abundance and show LREE enrichments (cryptic metasomatism). The La/Yb ratios range between 7 and 15 and Sm = 1.5–2 times chondrite. Due to higher clinopyroxene contents, the REE are more enriched in the lherzolite and wehrlite xenoliths (La/Yb ratio = 1.4–5.4 and Sm = 3.5–10 times chondrite).

7. P-T estimates

A number of geothermometers have been proposed that are applicable to the investigated xenoliths (e.g., Wells, 1977; Mercier, 1980; Lindsley, 1983; Brey and Koehler, 1990). Two of mostly recognized are the two-pyroxene geothermometer of Wells (1977) and of Brey

Table 7
Major and trace element analysis of basanites

Area	Muscat						Average	
Sample	Mb-1	Mb-2	Mb-3	Mb-4	Mb-5	Mb-6	Muscat	Al Ashkharah
SiO_2	41.95	42.15	42.89	42.32	42.41	42.38	42.35±0.32	43.27±0.68
TiO_2	1.90	2.05	2.12	2.25	2.16	1.95	2.07±0.13	2.19±0.08
Al_2O_3	11.80	12.13	12.43	11.85	11.91	12.28	12.07±0.13	13.43±0.36
Fe_2O_3	3.72	2.92	3.24	3.38	3.41	2.75	3.24±0.35	3.32±0.86
FeO	7.03	7.64	7.43	7.63	7.14	7.38	7.38±0.25	6.98±0.66
MnO	0.15	0.16	0.15	0.17	0.16	0.17	0.16±0.01	0.18±0.01
MgO	14.29	14.03	13.82	14.41	13.71	14.55	14.14±0.33	11.37±0.76
CaO	10.63	10.41	9.72	10.36	10.85	10.33	10.38±0.38	10.00±0.38
Na_2O	2.48	2.64	2.34	2.18	2.84	2.55	2.51±0.23	4.28±0.24
K_2O	1.38	1.44	1.29	1.32	1.51	1.48	1.40±0.09	1.78±0.26
P_2O_5	0.77	0.88	0.79	0.92	0.96	0.95	0.88±0.08	0.90±0.09
LOI	3.13	2.91	3.02	2.65	2.45	3.15		
Total	99.23	99.36	99.24	99.44	99.51	99.72		
Mg#	0.71	0.71	0.70	0.70	0.70	0.72	0.71±0.01	0.67±0.13
D.I.	18.1	19.08	19.61	16.64	20.62	18.67		
CIPW-norm								
Or	–	–	7.92	–	–	–		
Ab	–	–	1.19	–	–	–		
An	17.67	17.61	20.36	19.26	15.74	18.21		
Ne	11.83	12.55	10.50	10.36	13.41	12.06		
Di	25.31	23.81	19.35	21.91	26.34	22.50		
Ol	22.90	23.99	24.61	24.68	21.23	25.18		
Trace elements (ppm)								
V	164	173	160	188	175	165	174.1±9.1	198.6±1.4
Cr	405	395	380	425	360	440	400.8±29.2	364.8±65.4
Co	60	58	56	65	52	64	59.1±4.9	–
Ni	402	360	355	390	320	410	372.8±34.1	298.6±44.9
Rb	26	24	28	25	22	27	25.30±2.1	28.46±10.4
Sr	903	835	712	935	962	810	860±92.6	944.6±115.5
Zr	181	197	201	206	210	215	201±11.9	222.6±19
Y	18	20	22	22	24	24	21.6±2.3	22.9±1.7
Sc	27	25	28	24	29	26	26.5±1.87	–
Nb	95	98	101	103	91	96	97.3±4.3	88.4±6.6
Ba	1149	1018	950	1210	845	1180	1058±145	741.8±60.4
La	51.0	53.86	51.86	56.5	58.8	61.2	55.5±4.0	58.2±8.4
Ce	91.o	98.6	91.3	106.3	108.9	111.4	101.25±8.92	102.1±11.6
Nd	41.7	41.6	39.1	42.1	43.7	44.3	42.1±1.8	41.98±3.04
Sm	7.07	8.01	7.84	7.32	7.61	8.11	7.66±0.41	7.67±4.0
Eu	2.32	2.33	2.28	2.39	2.42	2.48	2.37±0.07	2.38±0.08
Tb	0.94	0.93	0.89	0.94	0.87	0.85	0.9±0.04	0.93±0.04
Dy	4.69	4.98	5.09	5.11	4.92	5.13	–	–
Yb	1.78	1.71	1.69	1.74	1.77	1.8	1.75±0.04	1.76±0.06
Lu	0.24	0.23	0.23	0.25	0.25	0.26	0.24±0.01	0.25±0.01
Th	10	11	12	10	13	11	11.1±1.1	7.94±1.52
U	2	3	2	2	4	2	2.5±0.8	–
Sm/Nd	0.1025	0.1160	0.1211	0.1051	0.1052	0.1106	0.1131±0.007	0.1095±0.003
$^{143}Nd/^{144}Nd$	0.51278	0.51275	0.51272	0.51274	0.51277	0.51272	0.51275±0.0004	0.51287±0.00003
$^{87}Sr/^{86}Sr$	0.70418	0.70411	0.70409	0.70415	0.70400	0.70408	0.70410±0.0001	0.70365±0.003
εNd	2.83	2.28	1.58	2.01	2.65	1.66	2.17±0.51	4.44±0.6

and Koehler (1990). Table 9 shows the temperatures obtained for the xenoliths using the above geothermometers calculated for a pressure of formation of 15 kbar. The estimated temperatures for the xenoliths from central and eastern Oman are relatively similar. The range in equilibrium temperatures obtained using the Wells' two PYX geothermometer is 950 to 1045 +50 °C, whereas that obtained using the Brey and

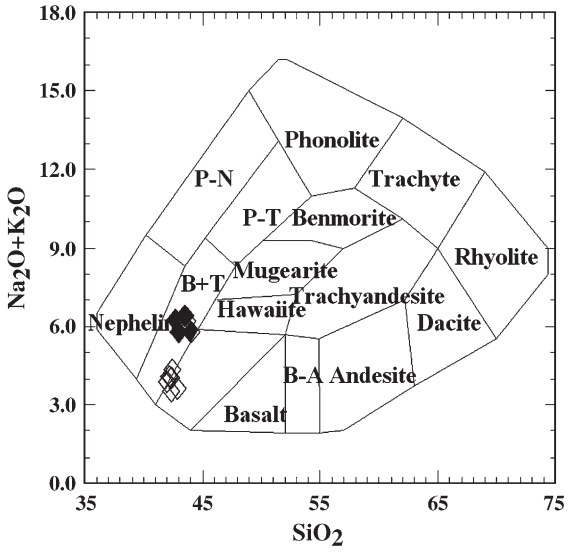

Fig. 2. Total alkalis versus silica plot for the Omani alkaline intrusions. (♦) Muscat area (◇) Al Ashkharah area. P-N = Phonolitic Nephelinites; P-T = Phonolitic Tephrite; B + T = Basanite and Tephrite; B-A: Basaltic Andesite. Data for Al Ashkharah basanites are from Worthing and Wilde (2002).

Koehler two PYX geothermometer is 910 to 1045 +50 °C. Relatively similar temperatures (905–990 °C) are obtained using the Ca content in orthopyroxene geothermometer of Brey and Koehler (1990). The estimated temperatures of equilibration are typical of basalt-hosted spinel lherzolites in general (e.g., Principalle et al., 1994).

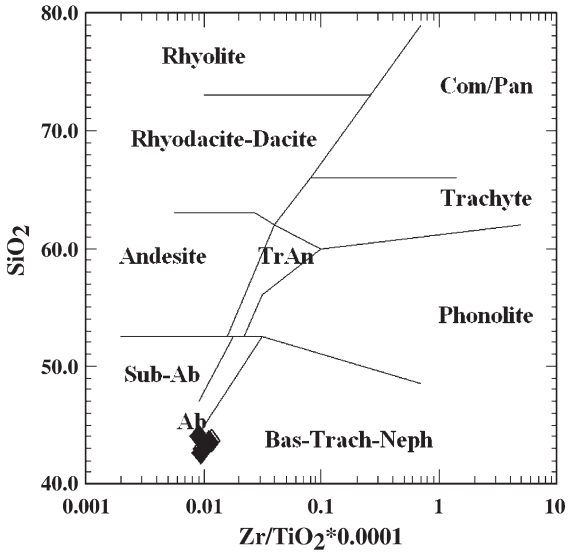

Fig. 3. SiO_2 versus Zr/TiO_2 classification diagram (Winchester and Floyd, 1976). Com/Pen = Comendite/Pantellerite; TrAn = Trachy Andesite; Sub-Ab = Sub-alkali basalt; Bas–Trach–Neph = Basanite–Trachyte–Nephelinite. Data for Al Ashkharah basanites are from Worthing and Wilde (2002). Symbols same as in Fig. 2.

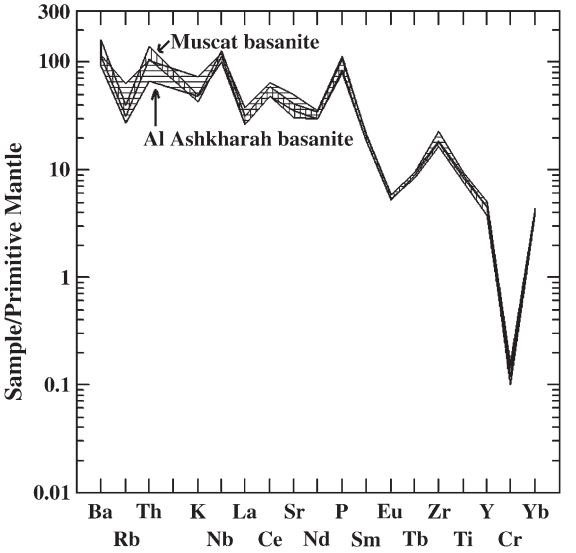

Fig. 4. Primitive mantle normalized trace element abundances in basanites from central Oman. Data of Al Ashkharah basanites are from Worthing and Wilde (2002). Normalizing values from Sun and McDonough (1989).

Pressure estimates in spinel lherzolites are difficult, and in general the errors on the estimates are typically as large as the spinel lherzolite filed. However, rough pressure estimates may be obtained by comparing the observed mineral assemblage to phase stability fields determined for plagioclase-, spinel- and garnet

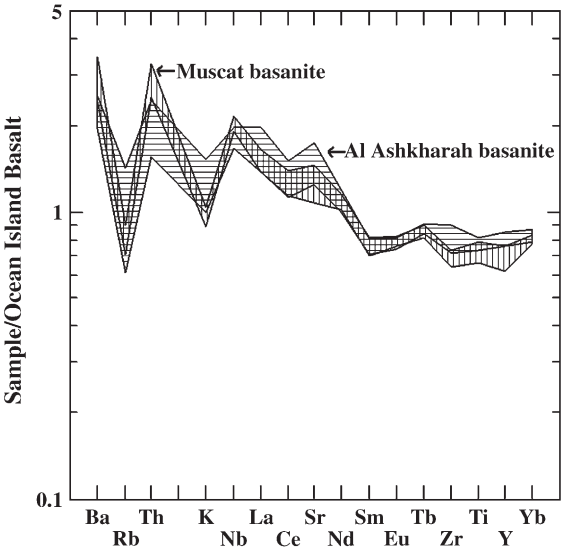

Fig. 5. Ocean island normalized trace element abundances in basanites from central Oman. Data of Al Ashkharah basanites are from Worthing and Wilde (2002). Normalizing values are from Sun and McDonough (1989).

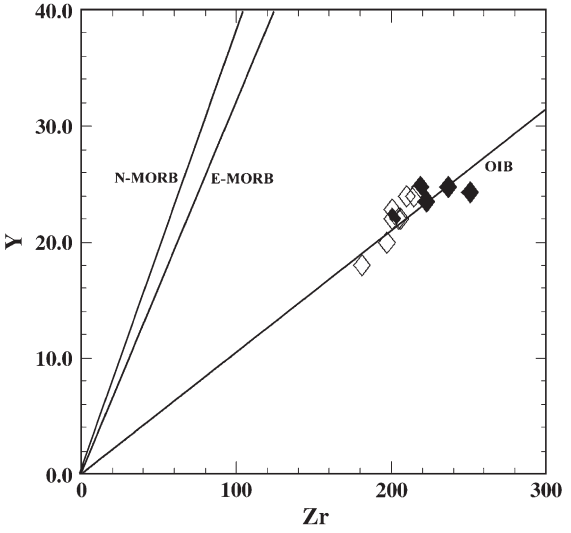

Fig. 6. Y versus Zr plot for basanites from central and eastern Oman. N-MORB, E-MORB and OIB are from Sun and McDonough (1989).

peridotites (Green and Hibberson, 1970; O'Hara et al., 1971). The mineral assemblage of the Omani xenoliths indicates a pressure range of 12–18 kbar (40–60 km depth) if the FeO contents of coexisting olivine (Fo_{90}) are accounted for (O'Neill, 1981). However, despite the low Ca content of olivine in the investigated xenoliths (<0.1 wt.%), application of the Ca in olivine geobarometer of Koehler and Brey (1990) yielded a pressure range of 12.7 to 19 kbar. The Cr in spinel geobarometer of O'Neill (1981) yielded a constant pressure of ~20 kbar in all samples. Fig. 11 shows the pressure–temperature estimates in comparison to the xenoliths geotherm of the Arabian plate.

8. Oxygen fugacity

Various oxybarometers have been widely applied to spinel peridotite xenoliths as a method to estimate the redox state of the upper mantle (e.g., Ballhaus, 1993; O'Neill and Wall, 1987; Wood, 1990). We have used the oxygen barometer of O'Neill and Wall (1987) to calculate oxygen fugacities for the Omani xenoliths. Calculated oxygen fugacities (Table 9) are given relative to the FMQ (fayalite–magnetite–quartz) buffer at 15 kbar. Oxygen fugacity is little affected by errors in determining ferric iron of spinel from electron microprobe data and has not changed substantially with direct determination of Fe^{3+} in spinel (e.g., Mattioli et al., 1989; Ballhaus, 1993; Nasir et al., 1993; Nasir, 1996). Oxygen fugacities of the Oman xenoliths fall in a relatively narrow range below the FMQ ($\Delta \log fO_{2FMQ} = -0.4$ to -2.2). The xenoliths from the Muscat area (central Oman) are more oxidized than those from the Ashkera area (southeast Oman) ($\Delta \log fO_{2FMQ} = -0.4$ to -0.9 and -1.1 to -2.2, respectively). These values are within the range for continental xenoliths from the northern parts of the Arabian plate (Nasir et al., 1993).

9. Discussion

High compatible trace element (Ni, Cr, V, Sc) concentrations, high Mg-numbers and the common occurrence of mantle xenoliths suggest that the Omani Tertiary basanites may be close to primary mantle melts. The trace element and Sr–Nd isotopic characteristics of the Oman Tertiary basanite areas consistent with their being derived from mantle sources with OIB-like trace element and isotopic characteristics (Figs. 5,6,8). Major and trace element variations in basanites and xenoliths from both central and southeastern Oman show striking similarities, indicating a common mantle source area.

A large body of experimental evidences demonstrates the dependence of the bulk composition of primary mantle melts on pressure (e.g., Kushiro, 1968; Jaques and Green, 1980) and suggests that silica undersaturated and alkaline magmas, such as the Tertiary Omani basanites, originate from the asthenosphere. Equations that relate bulk rock SiO_2 contents to the pressure of melting based on peridotite melting experiments have been suggested by several workers (e.g., Scarrow and Cox, 1995; Haase, 1996) and applied to estimate the depth of basaltic magma sources. The Omani basanites have about 42–43 wt.% SiO_2 (excluding contamination by xenocrysts) and these values

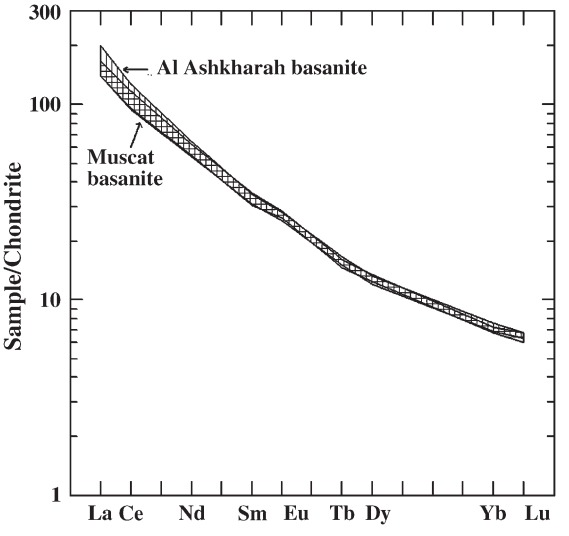

Fig. 7. Chondrite normalized rare earth element abundances in basanites. Normalizing values from Sun and McDonough (1989).

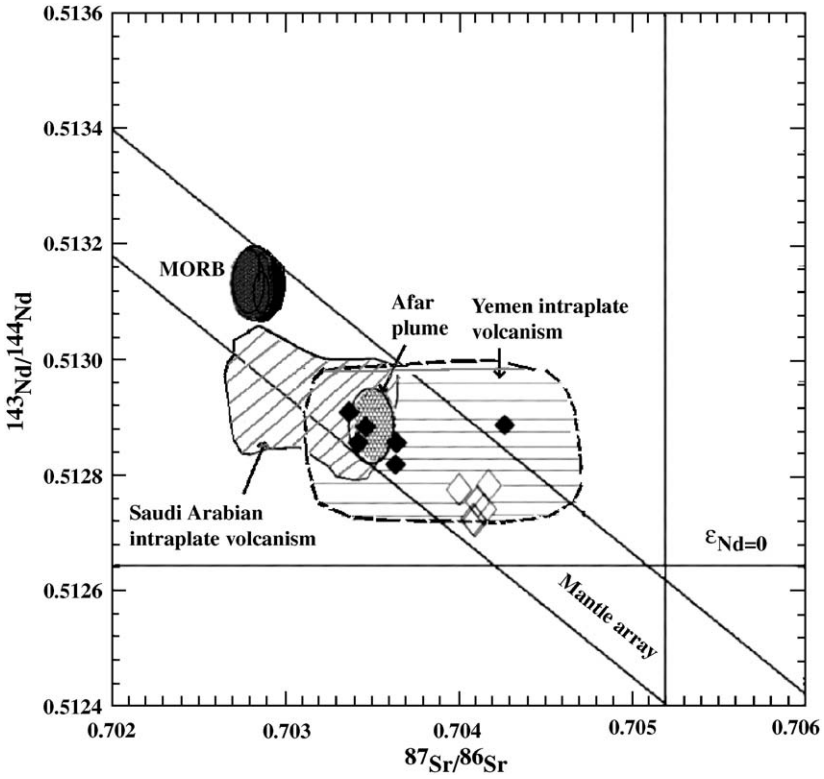

Fig. 8. Sr–Nd isotope variation in Tertiary basanites of central and eastern Oman. Data of Al Ashkharah basanites are from Worthing and Wilde (2002). Sources of the fields as follows: Afar plume, Arabian basalts, MORB and Yemen basalts after Baker et al. (1997). Data of Al Ashkharah basanites are from Worthing and Wilde (2002). Symbols same as in Fig. 2.

correspond to pressures of 45 to 50 kbar. Assuming a thickness of 40 km for the continental crust (Al-Lazki et al., 2002; Al-Damegh et al., 2005) with an average density of 2.8 g/cm^3, and a density of 3.3 g/cm^3 for the upper mantle, pressure of 40–50 kbar correspond to depths of roughly 130–160 km. Longmuir et al. (1992) found that the FeO_{total} contents of primary mantle vary with the pressure of melting. The basanite FeO_{total} contents of ~10 wt.% are consistent with an onset of melting at a minimum of 30 kbar (~100 km depth).

Mantle melting at depths below ~80 km is likely to involve garnet lherzolite in the asthenosphere and to produce melts relatively depleted in the heavy REE. The chondrite ratios of Sm/Yb in the Omani basanite are 4 to 5, and these values are consistent with the initiation of melting in the presence of residual garnet (McKenzie and O'Nion, 1991; Ellam, 1992). Trace element ratio plots provide important constraints for the relative roles of garnet- and spinel-bearing lherzolite mantle sources (Baker et al., 1997). In Fig. 12 melt modeling using the plots of Ce/Y versus Zr/Nb (Fig. 12a), La/Yb versus Yb (Fig. 12b), Zr/Sm/ versus Ce/Y (Fig. 12c) and Dy/Yb versus La/Yb (Fig. 12d) indicates that the incompatible trace element signature of the Omani volcanic rocks is consistent with the garnet-facies mantle source of the magmas (e.g., asthenospheric mantle). The ratios of Ce/Y, Zr/Sm, Zr/Nb and La/Yb show small variations (Fig. 12) and suggest that the Omani basanites are the product of ca 5% partial melting in the garnet field within the asthenosphere. However, a plot of Dy/Yb versus La/Yb (Fig. 12d) indicates that mixing of melts from both spinel- and garnet lherzolite-facies mantle (0.7 gt:0.3 sp) is likely to have occurred in the petrogenesis of the Omani Tertiary basanites. Spinel-facies melting produces little changes in Dy/Yb and La/Yb compared to the original mantle protolith. In contrast, garnet-facies melting produces large changes in Dy/Yb with melt fraction and the melt ratio is very different from the source ratio (1.07; Baker et al., 1997). In this diagram mixing of melts from spinel- and garnet-facies mantle domains will create linear arrays as indicated. This mixing might have occurred during diapiric mantle upwelling and/or due to remelting of a metasomatized spinel peridotite-facies mantle protolith which was derived by partial melting of garnet-facies mantle at deeper levels within the asthenosphere (~100 km).

Table 8
Major and trace element composition of xenoliths

Area	Muscat		Al Ashkharah								Average[a]
Rock	Dunite		Lherzolite		Wehrlite	Dunite		Wehrlite			Peridotite
Sample	Md-1	Md-2	Ml-1	Ml-2	Mw-3	Ad-1	Ad-2	Aw-1	Aw-2	Aw-3	
SiO_2	41.91	41.52	42.79	43.01	42.92	41.04	41.33	42.51	42.45	42.44	45.13
TiO_2	0.02	0.03	0.14	0.15	0.17	0.04	0.07	0.16	0.17	0.19	0.22
Al_2O_3	0.67	0.55	0.84	0.90	0.95	0.72	0.63	0.63	0.94	1.03	3.97
FeO_{tot}	8.97	8.80	9.60	9.50	9.11	9.77	9.71	9.11	8.87	8.76	7.82
MnO	0.14	0.16	0.35	0.41	0.44	0.19	0.17	0.47	0.42	0.44	0.13
MgO	46.66	47.33	42.81	42.1	41.96	46.16	46.72	43.64	43.55	43.84	38.3
CaO	1.51	1.24	3.06	3.37	3.87	1.63	1.06	3.02	2.9	2.71	3.50
Na_2O	0.10	0.15	0.19	0.22	0.24	0.12	0.09	0.22	0.23	0.26	0.33
K_2O	0.01	0.01	0.02	0.03	0.03	0.01	0.01	0.02	0.02	0.02	0.03
P_2O_5	0.01	0.01	0.01	0.01	0.01	0.01	0.01	0.01	0.01	0.01	
LOI	0.03	0.05	0.02	0.04	0.05	0.02	0.04	0.02	0.04	0.03	
Total	99.94	99.84	99.83	99.74	99.75	99.71	99.84	99.81	99.6	99.73	99.43
Mg#	0.90	0.90	0.89	0.90	0.89	0.89	0.90	0.90	0.90	0.90	90.0
V	44	52	33	32	30	39	42	35	28	31	
Cr	3980	3585	2370	2280	2200	4450	4120	2440	2550	2330	
Ni	2580	2240	1540	1490	1420	2430	2180	1160	1450	1360	
Rb	5	6	7	7	9	8	5	9	8	8	
Sr	22	30	35	38	42	24	28	36	44	48	
Sc	7.2	8.1	9.3	9.15	9.58	8.4	7.8	9.45	9.95	8.89	
Zr	13	15	55	62	69	14	14	31	38	42	
Y	2	3	4	6	5	3	2	6	5	4	
Nb	3	2	5	8	9	2	2	7	6	9	
La	1.83	1.25	2.04	2.45	6.9	2.04	2.45	4.15	4.66	3.86	
Ce	3.14	2.51	15.87	14.53	14.07	3.78	3.95	8.24	8.9	7.82	
Nd	2.06	1.61	10.58	9.31	8.35	2.12	2.23	4.91	5.07	4.82	
Sm	0.39	0.31	2.19	1.89	1.76	0.35	0.34	0.94	1.11	0.85	
Eu	0.09	0.07	0.49	0.42	0.38	0.1	0.12	0.28	0.31	0.24	
Tb	0.05	0.04	0.3	0.27	0.25	0.045	0.048	0.17	0.19	0.15	
Yb	0.24	0.17	1.43	1.24	1.7	0.15	0.16	0.77	0.91	0.75	
Lu	0.035	0.028	0.21	0.17	0.16	0.025	0.026	0.12	0.13	0.11	

[a] Average of upper mantle peridotite (Jagoutz et al., 1979).

Model melting curves for amphibole-bearing spinel and garnet lherzolite (Fig. 12c) do not suggest the involvement of significant amphibole in the mantle source region. Mixing of small degree melts (<2%) and larger degree melts (~5%) from garnet- (deep) and spinel-facies (shallow) mantle, respectively, can account for the observed REE data of the Omani Tertiary basanites (see also Baker et al., 1997). Worthing and Wilde (2002) suggest an ultimate origin of the Cenozoic basanites in southeast Oman through a small degree partial melting (2–5%) of garnet lherzolite.

Sr–Nd data show that the Omani volcanic rocks extend to higher $^{87}Sr/^{86}Sr$ and lower $^{143}Nd/^{144}Nd$ ratios (Fig. 8), a feature that is shared by Quaternary intraplate alkali volcanism from Yemen (Baker et al., 1997). However, the primitive composition and restricted range in incompatible elements and in Sr and Nd isotopic composition ($^{87}Sr/^{86}Sr = 0.70336–0.70426$, $^{143}Nd/^{144}Nd = 0.512719–0.512914$) of the Omani basanites indicate that the continental crust was not involved in their genesis. Part of the Omani samples (Al Ashkharah basanite) overlap with the isotopic composition of the Afar plume and Oligocene flood volcanism in Yemen (Baker et al., 1997; Kent et al., 2002). In comparison with Red Sea, Gulf of Aden (local MORB) and the Saudi Arabian intraplate basalts, the Omani Tertiary basanites clearly extend to more enriched isotopic composition. Bertrand et al. (2003) observed also that the southern Arabian Tertiary basalts (e.g., Yemen) have higher $^{87}Sr/^{86}Sr$ and lower $^{143}Nd/^{144}Nd$ ratios than those of the northern parts of the Arabian plate (Saudi Arabia, Jordan and Syria). These differences are believed to reflect heterogeneous development of the Arabian lithosphere through result from the thermal effect of the Afar plume on the southern part of the Arabian lithosphere (Bertrand et al., 2003). Generally, the Tertiary lava fields of the Arabian plate formed in two phases; the first phase occurred between 16 and

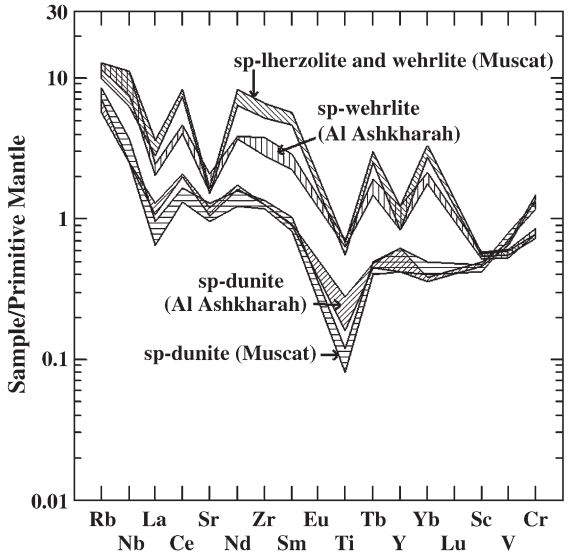

Fig. 9. Primitive mantle normalized trace element abundances for xenoliths from central and eastern Oman. Normalizing values from Sun and McDonough (1989).

24 Ma ago, and the second younger phase took place between 8 Ma and slightly less than 0.4 Ma (Camp and Roobol, 1989; Mouty et al., 1992; Nasir, 1994). They are related to the two-stage formation of the Red Sea and the Dead Sea rifts (Bohannon et al., 1989; Nasir, 1994; Baker et al., 1997). Several investigators concluded, through a substantial amount of isotopic data for the volcanic rocks from the Arabian Peninsula, that the primary magmas were derived from a shallow mantle source (<80 km (e.g., Altherr et al., 1990; Stein and Hoffman, 1992; Baker et al., 1997; Nasir and Safarjalani, 2002). Geochemical investigations of these volcanic rocks indicate that they were generated in response to the interaction of a rising fossil mantle plume with the surrounding lithosphere (Stein and Hoffman, 1992; Stein and Goldstein, 1996; Volker et al., 1997; Kent et al., 2002; Bertrand et al., 2003; Hopp et al., 2004). On regional scale, the Tertiary was a period of intense mantle plume activity (Stein and Hoffman, 1992). The Tertiary magmatism of Oman could, therefore, be a reflection of the same convective instability in the mantle that led to widespread intra-continental rifting in the Arabian plate. However, the timing (36 to 44 Ma) and the source of Omani Tertiary volcanism (a depth of ~100 km) is more likely to be the result of separate mantle upwelling or reactivation during Tertiary tectonism. The domal uplift and concurrent erosion of the basement in Jebel Ja'alan area, eastern Oman, are related to the upwelling of a contemporaneous mantle plume (Shackleton et al., 1990). This may reflect the presence of hotter than ambient mantle beneath the lithosphere in eastern Oman. There is some evidence for the existence of several fossil plumes underlying the Oman region. Continental break-up of eastern and central Oman in Permian time was initiated along a triple junction linking two directions; one that parallels the present east coast of Oman and the other along a NW–SE direction (Mountain and Prell, 1999). Al-Belushi et al. (1996) suggested that this triple junction was the locus of strong thermal uplift that elevated the eastern and central Oman areas. A mantle plume centered beneath this triple junction could have been the case of such uplift. However, alkaline volcanic activity was associated with each new rifting phase in the Neo-Tethys. Volcanics of the Middle Ordovician (Oterdoom et al., 1999), the Middle Permian (Lapierre et al., 2004) and of the Cretaceous of Oman (Glennie et al., 1974; Wyns et al., 1992; Peters et al., 2001) exhibit trace element and isotopic characteristics of plume-related magmas. The basanite magmas may have been derived by decompressional melting of these plume head due to minor lithospheric extension in Tertiary. However, the basanites intrusions of eastern Oman were coeval with deepening of the Abat trough due to Middle to Late Eocene reactivation of the Ja'alan fault (Al-Sayigh, 1998). Sediments were deposited in the Abat trough during Early Paleocene to Early Oligocene in a series of shallowing-upward cycles suggesting pulsed tectonic instability in local extensional tectonic regime (Filbrandt et al., 1990). Carbon (1996) indicates the absence of regional tectonic extension in the Eocene for Oman,

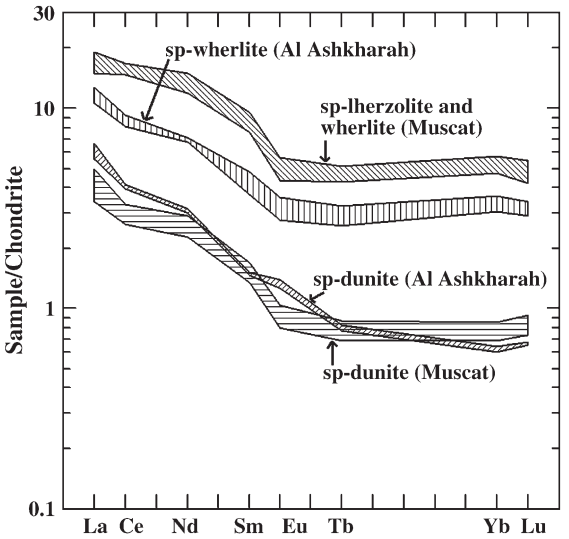

Fig. 10. Chondrite normalized rare earth element abundances for xenoliths from central and eastern Oman. Normalizing values from Sun and McDonough (1989).

Table 9
P-T estimates

Area	Muscat					Al Ashkharah				
Rock	Dunite		Lherzolite		Wehrlite	Dunite		Wehrlite		
Sample	Md-1	Md-2	Mw-1	Mw-2	Mw-3	Ad-1	Ad-2	Aw-1	Aw-2	Aw-3
Temperature (°C)										
W	955	990	1035	940	1045	975	960	955	975	950
BK	925	990	1020	910	1045	975	960	955	970	955
Ca (BK)	955	945	920	940	940	975	990	975	915	905
Pressure (kbar)										
Ca(ol)	17	19	18	15	14	16.1	12.7	13.5	17.4	15.3
Cr-Sp	20.5	20.3	20.6	20.8	20.7	20.4	20.2	20.5	20.7	20.5
Oxygen fugacity										
O & W	−0.8	−0.43	−0.82	−00.9	−0.52	−1.72	−1.14	−1.85	−1.36	−2.2
	−12.24	−10.44	−14.25	−12.71	−9.49	−13.2	−14.12	−12.64	−13.64	−9.39

W: Two pyroxene geothermometer Wells (1977), BK: Two-pyroxene geothermometer of Brey and Koehler (1990); Ca (BK): Ca in orthopyroxene geothermometer of Brey and Koehler (1990), Ca (ol): Ca in olivine geobarometer of Koehler and Brey (1990), Cr-Sp: Cr in spinel geobarometer of O'Neill (1981). O and W; oxygen barometer of O'Neill and Wall (1987).
Errors in estimated temperatures=+50 °C (e.g., Wells, 1977; Brey and Koehler, 1990).
The error bar for the Ca in olivine and Cr in spinel geobarometer is probably larger than the spinel lherzolite field.

although locally it may have occurred. The Tertiary basanites of Oman are clearly older than those of the Red Sea, which may indicate that the Tertiary alkaline magmatism in Oman is related with local extension. Gnos and Peters (2003) also related the Tertiary alkaline magmatism in Oman to local tectonic movements associated with plate reorganization in the Owens Basin region prior to the Red Sea opening.

The two mantle xenolith localities investigated belong to Type I (Frey and Green, 1974) or Cr-diopside series (Wilshire and Shervais, 1975) spinel peridotites, based on their petrography and mineral chemistry. The two xenolith occurrences show nearly complete overlap in their mineralogy, chemistry and calculated temperature of equilibration.

The mineralogy and chemistry of these xenoliths are similar to those found from mantle partial melting experimental studies (e.g., Jaques and Green, 1980). Therefore, they can be interpreted as residues from different degrees of partial melting. The LREE enrichment pattern is incompatible with a partial-melting model. This enrichment could be the result of late metasomatic addition components enriched in the incompatible trace elements.

The xenoliths from the Tertiary basanites indicate that the upper mantle below central and east Oman is more fertile than beneath other parts of the Arabian plate, where ol–cpx-rich dunite, lherzolite and wehrlite are dominant and harzburgites are absent. Formation of clinopyroxene and olivine at the expense of orthopyroxene is supported by their higher abundance in the Omani xenoliths than the northern Arabian plate. Progressive partial melting of peridotite at mantle pressures changes the phase assemblage of the residual rock from ol+opx+cpx+sp through ol+cpx+sp. Clinopyroxene is expected to be consumed when the residual rock contains 60–80% modal olivine (e.g., Jaques and Green, 1980). All mantle xenoliths form Oman contain >50% olivine and significant amounts of clinopyroxene. The modal proportions of clinopyroxene in these rocks thus appear to be dependent of olivine contents, strongly suggesting that the clinopyroxene is a part of residual assemblages.

Xenoliths from the western and northern parts of the Arabian plate comprise Group I spinel lherzolite and harzburgite and Group II pyroxenite, wehrlite, amphibole- and phlogopite-lherzolite and granulites (McGuire, 1988a,b; Nasir, 1992; Nasir and Safarjalani, 2002). In contrast to the granuloblastic textures prevalent amongst the Omani samples, the xenoliths from the northern and western parts of the Arabian plate have predominantly protogranular to porphyroblastic textures, and abundant evidence for mantle metasomatism (Nasir, 1992; Nasir and Safarjalani, 2002). The xenoliths from Oman rarely contains phlogopite and/or kaersutite and are likely to have been brought to the surface quickly after entrainment by the host magma, as the minerals do not exhibit any exsolution features (e.g., Huckenholz and Noussinanos, 1977). This contrasts strongly with the spinel peridotites from the northern and western parts of the Arabian plate, where extensive modal metasomatism (phologopite and kaersutite) is a

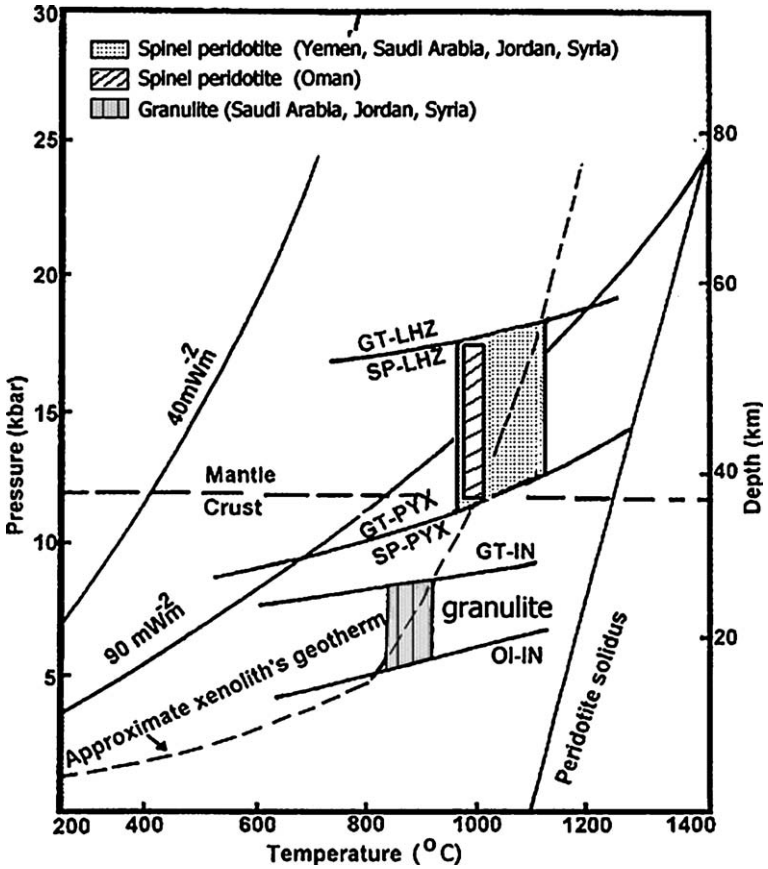

Fig. 11. Pressure–temperature estimates for the Omani xenoliths and approximate xenolith's geotherm of the Arabian plate modified after Nasir (1992) and Nasir and Safarjalani (2002). The spinel lherzolite (SP-LHZ)/garnet lherzolite transition is from O'Neill (1981). The spinel pyroxenite (SP-PYX)–garnet pyroxenite (GT-PYX) transition is from Herzberg (1978). The olivine-in (Ol-IN) and garnet-in (GT-IN) reactions are from Irving (1974). Dry peridotite solidus is from Ito and Kennedy (1971).

characteristic feature of the xenoliths as exsolution within the pyroxenes (Nasir, 1992; Nasir and Safarjalani, 2002). In similar contrast to the Arabian plate xenolith suite, lithologies such as Group II hydrous pyroxenite and lherzolites are also absent. Therefore, the mantle beneath the central and eastern parts of Oman (southeastern Arabian plate) has not experienced the metasomatism that appears prevalent to the northern and western parts of the Arabian plate.

The xenolith suite of central and eastern Oman Mountains records a relatively oxidized character. However, unlike the northern and western Arabian xenoliths, the Omani samples do not appear to have been affected by modal metasomatism which is seen to result in increased fO_2 for spinel peridotite from the northern and western parts of the Arabian plate (Nasir et al., 1993). The Omani xenoliths may therefore derived from a mantle that has experienced a different redox history from that of typical continental spinel peridotite of the northern and western parts of the Arabian plate. The upper mantle xenoliths from Oman show equilibrium temperatures between 910–1045+50 °C. The temperature–depth array recorded by the Omani xenoliths resembles that of many similar spinel peridotite suites from continental alkali basalts (Mercier, 1980) and from the Tertiary alkali basalts of the western and northern Arabian plate. If interpreted in a steady-state context, the mantle temperature translates to surface heat flux of ~90 mW m^{-2}. Similar temperatures are evident on a much larger scale within the xenolith suite of the Arabian plate (Nasir, 1992; Nasir and Safarjalani, 2002), testifying to the presence of a steady-state thermal condition within the Arabian plate.

Seismic and gravity data indicate that the eastern Arabian continental crust in Oman has an average thickness of about 40 km in the foreland region and is about 35 km beneath the coastal zone (Al-Lazki et al., 2002; Al-Damegh et al., 2004, 2005). The crust

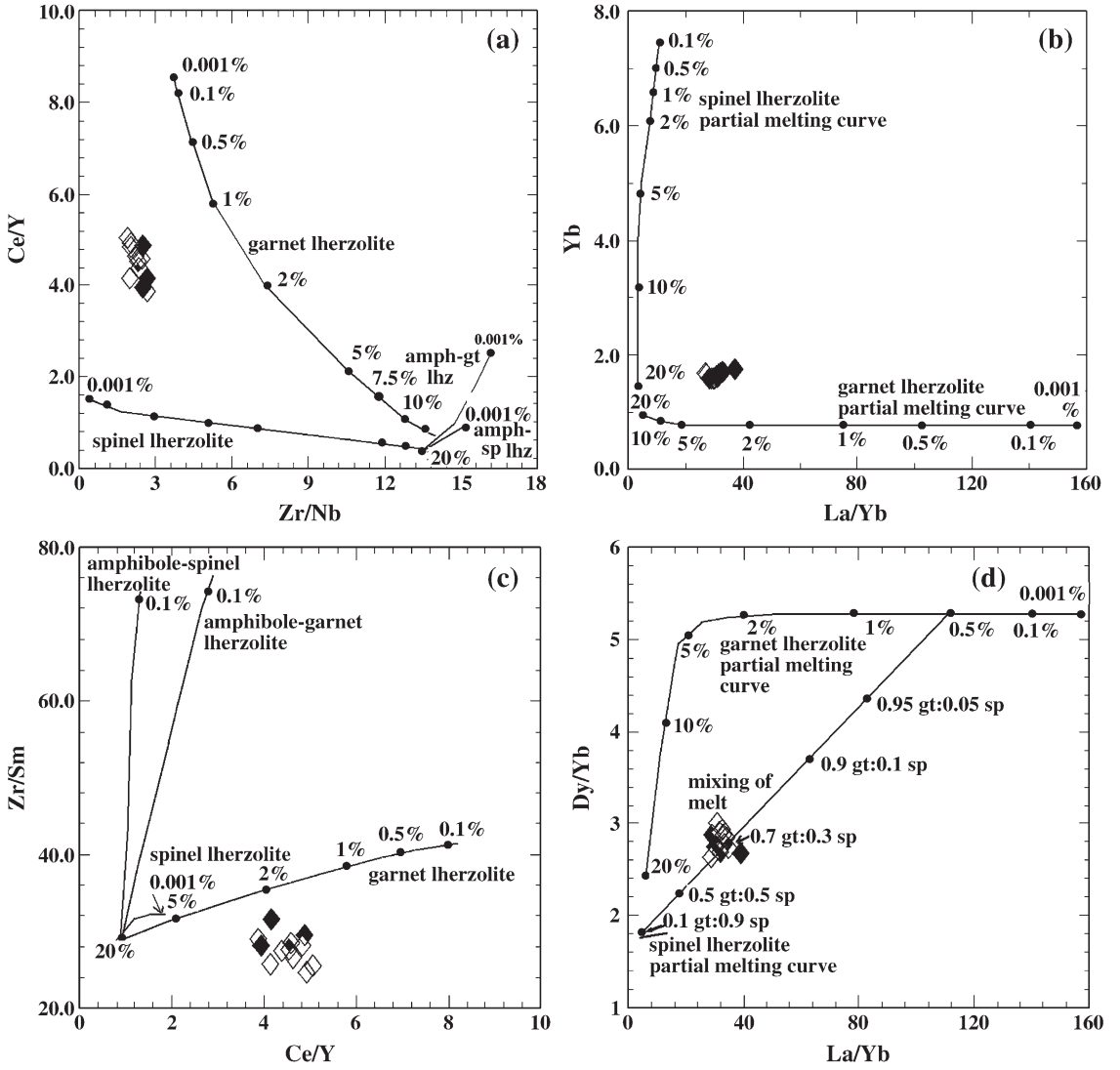

Fig. 12. a–d. Trace element ratio plots for the Omani basanites samples. (a) Ce/Y versus Zr/Nb, (b) Yb versus La/Yb, (c) Zr/Sm versus Ce/Y, and (d) Ce/Y versus Zr/Nb. Model melting curves for non-modal fractional melting of enriched mantle sources in the garnet (dashed) and spinel-facies mantle (solid) are from Baker et al. (1997). Degrees of melting along the model mantle melting curves are indicated in wt.%.

underneath the rift shoulder of Saudi Arabia has a thickness of 40 km, whereas the coastal plain has a crustal thickness of less than 20 km (Gettings et al., 1986). Seismic and gravity data indicate that the crust around the Harrat Ash Sham of Jordan and Syria is about 37 km thick (Ginzburg et al., 1979; El-Isa et al., 1987; McBride et al., 1990; Sawaf et al., 1993), and surface heat flows range from 52 to 54 mW m^{-2} (Matviyenko et al., 1993).

Fig. 13 shows a crust–mantle stratigraphic section derived for the Arabian lithosphere based on xenoliths and geophysical data. Gettings et al. (1986) predicted a temperature of about 450 °C at the base of the Arabian crust. This implies that the estimated geotherm is elevated in temperature above that of a stable continental shield. The higher xenolith temperatures suggest that the thermal gradient in the upper mantle is not in equilibrium with that at the surface. A temperature of 900 °C at 40 km depth intersects an equilibrated surface heat flow of about 90 mW m^{-2}. Estimated geotherms from other Arabian basalt provinces, Hutaymah (Thornber and Pallister, 1985), al Birk and al Kishb (McGuire, 1988a,b) and central Jordan (Nasir, 1992), south Syria (Nasir and Safarjalani, 2002) are similar to that of Oman. These data suggest that regional elevation of the geotherm below the volcanic provinces in Arabia might

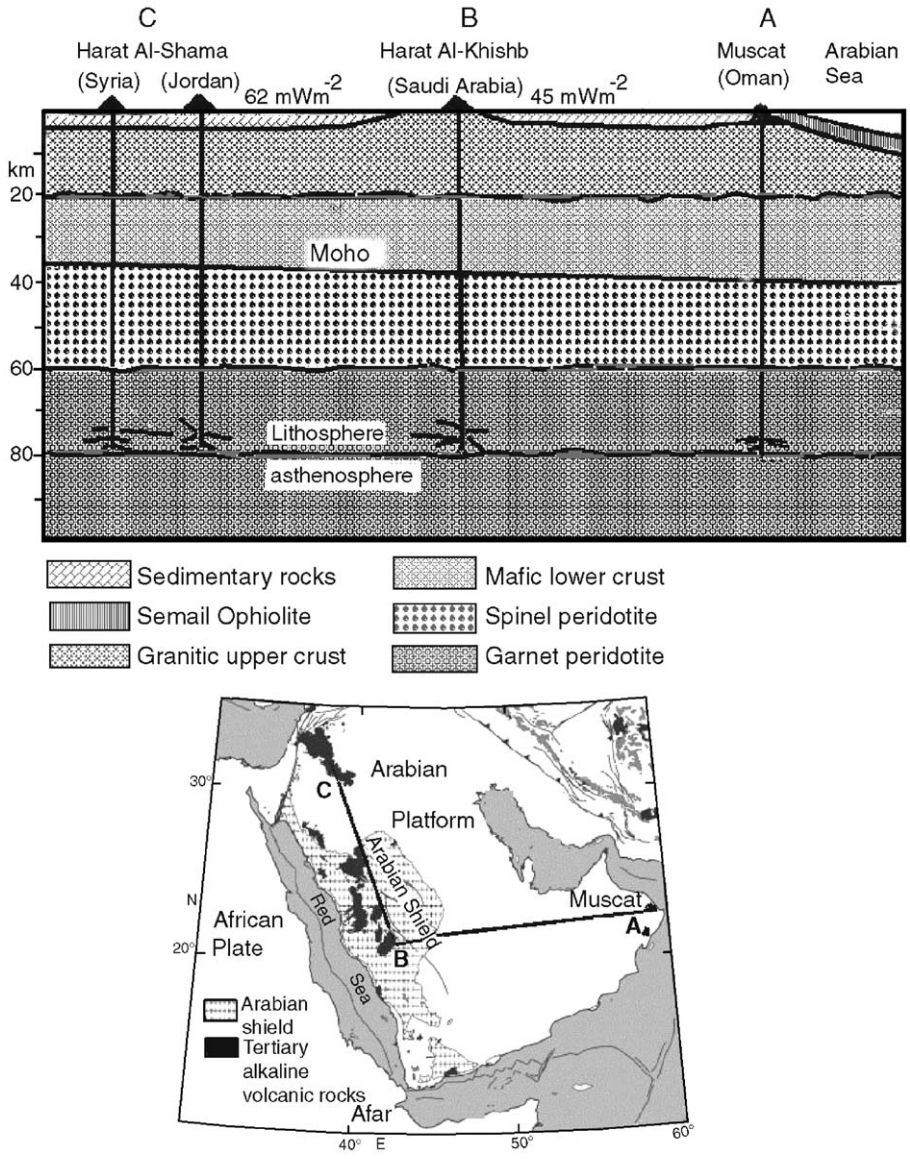

Fig. 13. Schematic cross-section of the Arabian plate. Heat flow from Gettings et al. (1986) and Matviyenko et al. (1993). Modified after Nasir and Safarjalani (2002).

be a widespread phenomenon. Heating may be due to intrusion of magma into the upper mantle and crust. Thinning of the Arabian lithosphere in times of extension may cause the thermal perturbations.

10. Conclusions

Mantle xenolith-bearing Tertiary basanites occur as small dikes and intrusions in the Muscat and Al Ashkharah areas. The basanites include primitive features with sttong OIB-like geochemical signatures. They occur along two main fault directions, approximately NS and E–W. The mantle xenoliths are mainly spinel dunite, spinel lherzolite and spinel wehrlite. The Omani mantle xenoliths seem different in types and chemistry and oxidation state to the related Yemen, Saudi Arabian, Syria, and Jordan mantle xenoliths. The present suite of mantle xenoliths from Oman indicate that the mantle beneath Oman is homogeneous on the small scale and moderately oxidized when compared with the xenolith suite from other parts of the Arabian plate. The timing, structural position and the source region of the Omani Tertiary basanites suggest that they were the result of melting asthenospheric mantle in

response to local Cenozoic lithospheric extension predating the Red Sea rift.

Acknowledgements

S. Nasir acknowledges financial support from the German academic exchange service (DAAD). Hans-Joachim Massonne and Thomas Theye are thanked for their help with the microprobe analysis. The authors thank Hugh Rollinson for reading early draft of the manuscript. The authors are grateful for the thorough and constructive reviews of T. Peters, E. Gnos and H. Lapierre.

References

Al-Belushi, J.D., Glennie, K.W., Williams, B.J., 1996. Permo-Carboniferous glaciogenic Al-Khalata Formation, Oman: a new hypothesis for origin of its glaciation. GeoArabia 1, 389–404.

Al-Damegh, K., Sandvol, E., Al-Lazki, A., Barazangi, M., 2004. Regional seismic wave propagation (Lg and Sn) and Pn attenuation in the Arabian plate and surrounding regions. Geophysical Journal International 157, 775–795.

Al-Damegh, K., Sandvol, E., Barazangi, M., 2005. Crustal structure of the Arabian plate: new constraints from the analysis of teleseismic receiver functions. Earth and Planetary Science Letters 231, 177–196.

Al Harthy, M.S., Coleman, R.G., Hughes-Clarke, M.W., Hanna, S., 1991. Tertiary basaltic intrusions in the central Oman Mountains. In: Peters, T.j., Nicolas, A., Coleman, G. (Eds.), Ophiolite Genesis and Evolution of the Oceanic Lithosphere, pp. 675–681.

Al-Lazki, A., Seber, D., Sandvol, E., Barazangi, M., 2002. A crustal transect across the Oman Mountains on the eastern margin of Arabia. GeoArabia 7, 47–78.

Al-Mishwat, A., Nasir, S., 2003. Composition of the lower crust of the Arabian Plate: a xenolith perspective. Lithos 72, 45–72.

Al-Sayigh, A. 1998. Lower Tertiary Formaminfera from South East Oman (Late Paleocene to Early Oligocene). PhD. Thesis, University of Wales, Aberyawyth. 248 pp.

Altherr, R., Henjes-Kunst, H., Baumann, A., 1990. Asthenosphere versus lithosphere as possible sources for basaltic magmas erupted during formation of the Red Sea: constraints from Sr, Pb and Nd isotopes. Earth and Planetary Science Letters 96, 269–286.

Baker, J.A., Menzies, M.A., Thirwal, M.F., McPherson, C.G., 1997. Petrogenesis of Quaternary intraplate volcanism, Sana'a Yemen: implications for plume–lithosphere interaction and polybaric melt hybridization. Journal of Petrology 38, 1359–1390.

Ballhaus, C., 1993. Redox states of lithospheric and asthenospheric upper mantle. Contributions to Mineralogy and Petrology 114, 331–348.

Béchennec, F., Roger, J., Chevrel, S., LeMetour, J.O.K., 1992. Explanatory Notes to the Geological Map of Al-Ashkerah, 1:250,000 Sheet NF 40–12. Directorate General of Minerals, Oman, Ministry of Commerce.

Bertrand, H., Chazot, G., Blichert-Toft, J., Thoral, S., 2003. Implications of widespread high-μ volcanism on the Arabian Plate for Afar mantle plume and lithosphere composition. Chemical Geology 198, 47–61.

Bohannon, R.G., Naeser, C.W., Schmidt, D.L., Zimmermann, R.A., 1989. The timing of uplift, volcanism, and rifting peripheral to the Red Sea: a case for passive rifting? Journal of Geophysical Research 94, 1683–1701.

Brey, G.P., Koehler, T., 1990. Geothermometry in four-phase lherzolites II. New thermobarometers, and practical assessment of existing thermometers. Journal of Petrology 31, 1353–1378.

Camp, V.E., Roobol, M.J., 1989. The Arabian continental alkali basalt province: Part I. Evolution of Harrat Rahat, Kingdom of Saudi Arabia. Geological Society of America Bulletin 101, 71–95.

Camp, V.E., Roobol, M.J., Hooper, P.R., 1991. The Arabian continental alkali basalt province: Part II. Evolution of Harrat Khaybar, Ithayn and Kura, Kingdom of Saudi Arabia. Geological Society of America Bulletin 103, 363–391.

Camp, V.E., Roobol, M.J., Hooper, P.R., 1992. The Arabian continental alkali basalt province: Part III. Evolution of Harrat Kishb, Kingdom of Saudi Arabia. Geological Society of America Bulletin 104, 379–396.

Carbon, D., 1996. Tectonique post-obduction des montagnes d'Oman dans le cadre de laconvergence Arabie-Iran. Sciences et Techniques du Languedoc. Universite Montpellier II, Montpellier, pp. 1–404.

Eggins, S.M., Rudnick, R.L, McDonough, W.F., 1998. The composition of peridotites and their minerals: a laser ablation ICP-MS study. Earth and Planetary Science Letters 154, 53–71.

El-Isa, Z., Mechie, J., Prodehl, C., Makris, J., Rihm, R., 1987. A crustal structure study of Jordan derived from seismic refraction data. Tectonophysics 138, 235–253.

Ellam, R.M., 1992. Lithosphereic thickness as a control on basalt geochemistry. Geology 20, 153–156.

Filbrandt, J.B., Nolan, S.C., Ries, A.C., 1990. Late Cretaceous and Early Tertiary evolution of Jebel Ja'alan and adjacent areas. In: Robertson, A.H.F., Searle, M.P., Ries, A. (Eds.), The Geology and Tectonics of the Oman Region. Geological Society of London Special Publications, vol. 49, pp. 697–714.

Frey, F.A., Green, D.H., 1974. The mineralogy, geochemistry and origin of lherzolite inclusions in Victorian basanites. Geochimica et Cosmochimica Acta 38, 1023–1059.

Frey, F.A., Prinz, M., 1978. Ultramafic inclusions from San Carlos, Arizona: petrologic and geochemical data bearing on their petrogenesis. Earth and Planetary Science Letters 38, 129–176.

Gautheron, C., Moreira, M., Allègre, C., 2005. He, Ne and Ar composition of the European lithospheric mantle. Chemical Geology 217, 97–112.

Gettings, M.E., Blank, H.R., Mooney, W.D., Healy, J.H., 1986. Crustal structure of Southwestern Saudi Arabia. Journal of Geophysical Research B91 (B6), 6491–6512.

Ginzburg, A., Makris, J., Fuchs, K., Prodehl, C., Kamisnki, W., Amital, U., 1979. A seismic study of the crust and upper mantle of the Jordan–Dead Sea Rift and their transition toward the Mediterranean Sea. Journal of Geophysical Research B84, 5605–5612.

Glennie, K.W., Boef, M.G.A., Hugues Clarke, M.W., Moody-Stuart, M., Pilaart, W.F.H., Reinhart, B.M., 1974. Geologie of the Oman Mountains. Verhandelingen van het Koninklijk Nederlands geologisch mijnbouwkundig Genootschap 31, 1–423.

Gnos, E., Peters, T., 2003. Mantle xenolith-bearing Maastrichtian to Tertiary akaline magmatism in Oman. Geochemistry, Geophysics, Geosystems (G-cubed) 4, 8620.

Green, D.H., Hibberson, W., 1970. The instability of plagioclase in peridotite at high pressure. Lithos 3, 209–221.

Griffin, W.L., O'Reilly, S.Y., 1987. The composition of the lower crust and nature of the continental Moho-xenolith evidence.

In: Nixon, P.H. (Ed.), Mantle Xenoliths. Wiley, Chichester, pp. 413–420.

Griffin, W.L., O'Reilly, S.Y., Ryan, C.G., 1999. The composition and origin of sub-continental lithospheric mantle. In: Fei, Y., Bertka, C. M., Mysen, B.O. (Eds.), Mantle Petrology: Field Observations and High-Pressure Experimentation. Special Publication, Geochemical Society of Houston, vol. 6, pp. 13–45.

Haase, K.M., 1996. The relationship between the age of the lithosphere and the composition of oceanic magmas: constraints on partial melting, mantle sources and the thermal structure of the plates. Earth and Planetary Science Letters 144, 75–92.

Hanna, S., 1990. The Alpinedeformation of the Central Oman Mountains. In: Robertson, A.H.F., Searle, M.P., Ries, A. (Eds.), The Geology and Tectonics of the Oman Region. Geological Society of London Special Publications, vol. 49, pp. 341–352.

Henjes-Kunst, F., Altherr, R., Baumann, A., 1990. Evolution and composition of the lithospheric mantle underneath the western Arabian Peninsula: constraints from Sr–Nd isotope systematics of mantle xenoliths. Contributions to Mineralogy and Petrology 105, 406–427.

Herzberg, C.T., 1978. Pyroxene geothermometry and geobarometry; experimental and thermodynamic evaluation of some subsolidus phase relations involving pyroxenes in the system CaO–MgO–Al_2O_3–SIO_2. Geochimica et Cosmochimica Acta 42, 945–958.

Hopp, J., Trieloff, M., Altherr, R., 2004. Neon isotopes in mantle rocks from the Red Sea region reveal large-scale plume–lithosphere interaction. Earth and Planetary Science Letters 219, 61–76.

Huckenholz, H.G., Noussinanos, T., 1977. Evaluation of temperature and pressure conditions in alkali basalts and their peridotite xenoliths in NE Bavaria, Western Germany. Neues Jahrbuch für Mineralogie Abhandlungen 129, 139–159.

Immenhauser, A., Schreuers, G., Peter, T., Matter, A., Hauser, M., Dumitrica, P., 1998. Stratigraphy, sedimentology and depositional environment of the Permain to uppermost Cretaceous Batain Group, eastern Oman. Eclogae Geologicae Helveticae 91, 217–235.

Ionov, D.A., Ashchepkov, I., Jagoutz, E., 2005. The provenance of fertile off-craton lithospheric mantle: Sr–Nd isotope and chemical composition of garnet and spinel peridotite xenoliths from Vitim, Siberia. Chemical Geology 217, 4175.

Irving, A.J., 1974. Geochemical and high pressure experimental studies of garnet pyroxenite and pyroxene granulite xenoliths from the delegate basaltic pipes, Australia. Journal of Petrology 15, 1–40.

Ito, K., Kennedy, G.C., 1971. An experimental study of the basalt–garnet granulite–eclogite transition. The Structure and Physical Properties of the Earth's Crust. Geophysical Monograph, vol. 14, pp. 303–314.

Jaques, A.L., Green, D.H., 1980. Anhydrous melting of peridotite at 0–15 kb pressure and the genesis of tholeiitic basalts. Contributions to Mineralogy and Petrology 73, 287–310.

Jagoutz, E., Palme, H., Baddenhausen, H., Blum, K., Cendales, M., Dreibus, G., Spettel, B., Lorenz, V., Waenke, H., 1979. The abundance of major, minor and trace elements in the earth's mantle as derived from primitive ultramafic nodules. Proceedings of the Lunar and Planetary Science Conference 10, 2031–2250.

Jenner, G.A., Longerich, H.P., Jackson, S.E., Freyer, B.J., 1990. ICP-MS — a powerful tool for high-precision trace element analysis in Earth sciences: evidence from analysis of selected U.S.G.S. reference samples. Chemical Geology 83, 133–148.

Karamalkar, N.R., Rege, S., Griffin, W.L., O'Reilly, S., 2005. Alkaline magmatism from Kutch, NW India: implications for plume–lithosphere interaction. Lithos 81, 101–119.

Kempton, P.D., Downes, H., Embey-Iszten, A., 1997. Mafic granulite xenoliths in Neogene alkali basalts from the western Pannonian basin, insight into the lower crust of a collapsed orogen. Journal of Petrology 38, 941–968.

Kent, A.R., Baker, J., Wiedenbeck, M., 2002. Contamination and melt aggregation processes in continental flood basalts: constraints from melt inclusions in Oligocene basalts from Yemen. Earth and Planetary Science Letters 202, 577–594.

Koehler, T.P., Brey, G.P., 1990. Calcium exchange between olivine and clinopyroxene calibrated as a geothermobarometer for natural peridotites from 2 to 60 kb with applications. Geochimica et Cosmochimica Acta 54, 2375–2388.

Kushiro, I., 1968. Composition of magmas formed by partial zone melting of the earth's mantle. Journal of Geophysical Research 73, 619–634.

Lapierre, H., Samper, A., Bosch, D., Maury, R.C., Bechennec, F., Cotton, J., Demant, A., Brunet, P., Keller, F., Marcoux, J., 2004. The Tethyan plume: geochemical diversity of Middle Permain basalts from the Oman rifted margin. Lithos 74, 167–198.

Laws, E.D., Wislon, M., 1997. Tectonics and magmatism associated with Mesozoic passive continental margin development in the Middle East. Journal of the Geological Society of London 154, 459–464.

Lindsley, D.H., 1983. Pyroxene thermometry. American Mineralogist 68, 477–493.

Longmuir, C., Klein, H., Plank, E.M., 1992. Petrological systematics of mid-ocean ridges. In: Morgan, J.P., Blackman, D.K., Sinton, J.M. (Eds.), Mantle Flow and Melt Generation at Mid-Ocean Ridges. American Geophysical Union, Washington, pp. 183–280.

Mann, A., Hanna, S., Nolan, S.C., 1990. The post-Campanian structural evolution of the Central Oman Mountains: Tertiary extension of the east Arabian margin. In: Robertson, A.H.F., Searle, M.P., Ries, A. (Eds.), The Geology and Tectonics of the Oman Region. Geological Society of London Special Publications, vol. 49, pp. 549–563.

Matviyenko, V.N., Makhan, K.O.M., Khazim, D., El-Khair, Y., Asmi, M., 1993. Geothermal conditions in oil- and gas-bearing regions of Syria. International Geology Review 35, 453–466.

Mattioli, G.S., Baker, M.B., Rutter, M.J., Stolper, E., 1989. Upper mantle oxygen fugacity and its relationship to metasomatism. Journal of Geology 97, 521–536.

McBride, J., Barazangi, M., Best, J., Al-Sad, D., Sawaf, T., Al-Tori, M., Gebran, A., 1990. Seismic reflection structure of intracratonic Palymyride fold-thrust belt and surrounding Arabian platform, Syria, The American Association of Petroleum Geology. Bulletin 74, 238–259.

McDonough, W.F., Frey, F.A., 1989. Rare earth elements in upper mantle rocks. In: Lipin, B.R., McKay, G.A. (Eds.), Geochemistry and Mineralogy of Rare Earth Elements. Mineralogical of Society America, Washington, pp. 99–145.

McGuire, A.V., 1988a. Petrology of mantle xenoliths from Harrat al Kishb: the mantle beneath Western Saudi Arabia. Journal of Petrology 29, 73–92.

McGuire, A.V., 1988b. The mantle beneath the Red Sea margin: xenoliths from western Saudi Arabia. Tectonophysics 150, 101–119.

McKenzie, D., O'Nion, R.K., 1991. Partial melt distribution from inversion of rare earth element concentrations. Journal of Petrology 32, 1021–1091.

Mercier, J.C.C., 1980. Single pyroxene thermobarometry. Tectonophysics 70, 1–37.

Mountain, G.S., Prell, W.L., 1999. A multiphase plate tectonic history of the southeast continental margin of Oman. In: Robertson, A.H. F., Searle, M.P., Ries, A. (Eds.), The Geology and Tectonics of the Oman Region. Geological Society of London Special Publications, vol. 49, pp. 725–744.

Mouty, M., Delaloye, M., Fontignie, D., Piskin, O., Wagner, J.J., 1992. The volcanic activity in Syria and Lebanon between Jurassic and Actual. Schweizerische Mineralogische und Petrographische Mitteilungen 72, 91–105.

Nasir, S., 1992. The lithosphere beneath the northwestern part of the Arabian plate Jordan. Evidence from xenoliths and geophysics. Tectonophysics 201, 357–370.

Nasir, S., 1994. Geochemistry and petrogenesis of Cenozoic volcanic rocks from the northwestern part of the Arabian continental alkali basalt province, Jordan. Africa Geoscience Review 1, 455–467.

Nasir, S., 1995. Cr-poor megacrysts from the Shamah volcanic field, northwestern part of the Arabian plate. Journal of African Earth Science 21, 349–357.

Nasir, S., 1996. Mafic lower crustal xenoliths from the northwestern part of the Arabian late. European Journal of Mineralogy 7, 217–230.

Nasir, S., Al-Fuqha, H., 1988. Spinel lherzolite xenoliths from the Aritain volcano, NE-Jordan. Mineralogy and Petrology 38, 127–137.

Nasir, S., Mahmood, S., 1991. Oxidation of olivine in lherzolitic xenoliths from NE-Jordan. Mu'tah Journal for Research and Studies 6, 171–182.

Nasir, S., Safarjalani, A., 2002. Lithospheric petrology and geochemistry beneath the Northern part of the Arabian Plate (Syria). Journal of African Earth Science 34, 223–245.

Nasir, S., Abu-Aljarayesh, I., Mahmood, S., Lehlooh, A., 1992. Oxidation state of the upper mantle beneath the northwestern part of the Arabian lithosphere. Tectonophysics 213, 359–366.

Nasir, S., Lehlooh, A., Abu-Aljarayesh, I., Mahmoodm, S., 1993. Ferric iron in upper mantle Cr-spinel, a Mössbauer spectroscopic study. Chemie der Erde 53, 265–271.

Neumann, E.R., Wulff-Pedersen, E., Pearson, N.J., Spencer, E.A., 2002. Mantle xenoliths from Tenerif (canary Islands): evidence for reactions between mantle peridotites and silicic carbonatite melts inducing Ca metasomatism. Journal of Petrology 43, 825–857.

Nolan, S.C., Clissold, B.P., Smewing, J.D., Skelton, P.W., 1990. Late Campanian to Tertiary paleogeography of the centran and northern Oman Mountains. In: Robertson, A.H.F., Searle, M.P., Ries, A. (Eds.), The Geology and Tectonics of the Oman Region. Geological Society, London, Special Publications, vol. 49, pp. 495–519.

O'Hara, M.H., Richardson, S.W., Wilson, G., 1971. Garnet peridotite stability and occurrence in crust and mantle. Contributions to Mineralogy and Petrology 32, 48–68.

O'Neill, H.S.C., 1981. The transition between spinel lherzolite and garnet lherzolite, and its use as a geobarometer. Contributions to Mineralogy and Petrology 77, 185–194.

O'Neill, H.S, Wall, V.J., 1987. The olivine–orthopyroxene–spinel oxygen geobarometer, the nickel precipitation curve, and the oxygen fugacity of the earth's upper mantle. Journal of Petrology 28, 1169–1191.

Oterdoom, H., Worthing, M.A., Partington, M., 1999. Petrological and tectonostratigraphic evidence for a mid Ordovician rift pulse on the Arabian Peninsula. Geoarabia 4, 467–500.

Peters, T., Al-Battashy, M., Bläsi, H., Hauser, M., Immenhauser, A., Moser, L., Al Rajhi, A., 2001. Explanatory notes to the geological maps of Sur and Al Ashkharah, Sheets NF 40-8F and NF 40-12C, scale 1: 100'000. Ministry of Commerce and Industry, Directorate General of Minerals, Muscat, Oman.

Princivalle, F., Salviulo, G., Fabro, C., Demarchi, G., 1994. Inter- and intra-crystalline temperature and pressure estimates on pyroxenes from NE Brazil mantle xenoliths. Contributions to Mineralogy and Petrology 116, 1–6.

Ries, A.C., Shackleton, R.M., Cunnigham, G.L., Lee, C.W., Skelton, P.W., 1985. A continuation of geological studies in the Batain Cost Region, NE Oman. Unpublished report, Amoco Petroelum Company.

Robertson, A.H.F., Searle, M.P., 1990. The Northern Oman Tethyan continental margin: stratigraphy, structure, concepts and controversies. In: Robertson, A.H.F, Searle, M.P., Ries, A.C. (Eds.), The Geology and Tectonics of the Oman Region. Geological Society of London Special Publications, vol. 49, pp. 3–25.

Rudnick, R.L., 1992. Xenoliths — samples of the lower continental crust. In: Fountain, D.M., Arculus, R., Kay, R.W. (Eds.), Coninental Lower Crust. Elsevier, pp. 269–316.

Sawaf, T., Al-Saad, D., Gebran, A., Barazangi, M., Best, A., Chiamov, T., 1993. Stratigraphy and structure of eastern Syria across the Euphrates depression. Tectonophysics 230, 267–281.

Scarrow, J.H., Cox, K.G., 1995. Basalts generated by decompressive adiabatic melting of a mantle plume: a case study from the Isle of Skye, NW Scotland. Journal of Petrology 36, 3–22.

Shackleton, R.M., Ries, A.C., A.C., Bird, P.R., Filbrandt, H.B., Lee, C. W., Cunningham, G.C., 1990. The Batain Melange of NE Oman. In: Robertson, A.H.F., Searle, M.P., Ries, A. (Eds.), The Geology and Tectonics of the Oman Region. Geological Society of London Special Publications, vol. 49, pp. 673–696.

Schilling, J.G., Kingsley, R.H., Hanan, B.B., McGully, B.L., 1992. Nd–Sr–Pb isotopic variations along the Gulf of Aden: evidence for mantle–plume–continental lithosphere interaction. Journal of Geophysical Research 97, 10927–10966.

Simonetti, A., Goldstein, S.L., Schmidberger, S.S., Viladkar, S.G., 1998. Geochemical and Nd, Pb, and Sr isotope data from Deccan Alkaline complexes—inferences for mantle sources and plume–lithosphere interaction. Journal of Petrology 39, 1847–1864.

Stein, M., Goldstein, S.L., 1996. From plume head to continental lithosphere in the Arabian–Nubian shield. Nature 382, 773–778.

Stein, M., Hoffman, A.W., 1992. Fossil plume head beneath the Arabian lithosphere? Earth and Planetary Science Letters 114, 193–209.

Stein, M., Navon, O., Kessel, R., 1997. Chromostratigraphic metasomatism of the Arabian Nubian lithosphere. Earth and Planetary Science Letters 152, 75–91.

Sun, S.S., McDonough, W.F., 1989. Chemical and isotopic systematics of oceanic basalts: implications for mantle composition and processes. Magmatism in the Ocean Basins. Geological Society of London, London, pp. 313–345.

Thornber, C.R., Pallister, J.S., 1985. Mantle xenoliths from northern Saudi Arabia. AGU 1985 Spring Meeting, Eos Transactions, American Geophysical Union, vol. 66, p. 393.

Trumbull, R.B., Buehn, B., Romer, R.L., Volker, F., 2003. The petrology of basanite–tephrite intrusions in the Erongo Complex and implications for a plume origin of Cretaceous alkaline complexes in Namibia. Journal of Petrology 44, 93–111.

Wells, P.A., 1977. Pyroxene thermometry in simple and complex systems. Contributions to Mineralogy and Petrology 62, 129–139.

Wilshire, H.G., Shervais, J., 1975. Al-augite and Cr-diopside series ultramafic xenoliths in basaltic rocks from western United States. Physics and Chemistry of the Earth 9, 257.

Wilson, M., Downes, H., 1991. Tertiary–Quaternary extension-related alkaline magmatism in Western and Central Europe. Journal of Petrology 32, 811–849.

Winchester, J.A., Floyd, P.A., 1976. Geochemical magma type discrimination; application to altered and metamorphosed basic igneous rocks. Earth and Planetary Science Letters 28, 459–469.

Wood, B.J., 1990. Oxygen barometry of spinel peridotites. In: Lindsley, D.H. (Ed.), Mineralogical Society of America. Reviews in Mineralogy, vol. 25, pp. 417–431.

Worthing, M., Wilde, A.R., 2002. Basanites related to Late Eocene extension from NE Oman. Journal of Geological Society of London 159, 469–483.

Wyns, R., Béchennec, F., Le Metour, J, F., Roger, J., Chevrel, S., 1992. Explanatory Notes to the Geological Map of Sur, 1:250,000 Sheet NF 40-08. Directorate General of Minerals, Oman, Ministry of Commerce.

Vannucci, R., Bottazi, P., Wulf-Pederson, E., Neumann, E.R., 1998. Naturally determined REE, Y, Sr, Zr and Ti partition coefficients between clinopyroxene and silicate melts under upper mantle conditions. Earth and Planetary Science Letters 158, 39–51.

Volker, F., Alther, R., Jochum, KP., McCulloch, M., 1997. Quaternary volcanic activity of the southern Red Sea: new data and assessment of models on magma sources and Afar plume–lithosphere interaction. Tectonophysics 278, 15–29.